Actionable Genetic Screens Unveil Targeting of AURKA, MEK, and Fatty Acid Metabolism as an Alternative Therapeutic Approach for Advanced Melanoma

JIDOpen

Federica Marocchi[1], Fernando Palluzzi[2], Paola Nicoli[1], Marine Melixetian[1], Giulia Lovati[1], Giovanni Bertalot[1,3,4], Salvatore Pece[1,5], Pier Francesco Ferrucci[1], Daniela Bossi[1,6] and Luisa Lanfrancone[1]

Despite the remarkable improvements achieved in the management of metastatic melanoma, there are still unmet clinical needs. A considerable fraction of patients does not respond to immune and/or targeted therapies owing to primary and acquired resistance, high-grade immune-related adverse events, and a lack of alternative treatment options. To design effective combination therapies, we set up a functional ex vivo preclinical assay on the basis of a drop-out genetic screen in metastatic melanoma patient-derived xenografts. We showed that this approach can be used to isolate actionable vulnerabilities predictive of drug efficacy. In particular, we highlighted that the dual targeting of AURKA and MAPK/extracellular signal–regulated kinase kinase employing the combination of alisertib and trametinib is highly effective in a cohort of metastatic melanoma patient-derived xenografts, both ex vivo and in vivo. Alisertib and trametinib combination therapy outperforms standard-of-care therapy in both *BRAF*-mutant patient-derived xenografts and targeted therapy-resistant models. Furthermore, alisertib and trametinib treatment modulates several critical cancer pathways, including an early metabolic reprogramming that leads to the transcriptional upregulation of the fatty acid oxidation pathway. This acquired trait unveiled an additional point of intervention for pharmacological targeting, and indeed, the triple combination of alisertib and trametinib with the fatty acid oxidation inhibitor etomoxir proved to be further beneficial, inducing tumor regression and remarkably prolonging the overall survival of the mice.

Journal of Investigative Dermatology (2023) ■, ■–■; doi:10.1016/j.jid.2023.03.1665

INTRODUCTION

In the last decade, the approval of targeted and immune therapies has revolutionized the treatment of advanced melanoma, providing significant clinical benefits (Larkin et al., 2019; Robert et al., 2019; Schadendorf et al., 2018). However, a considerable fraction of patients commonly experiences rapid development of secondary resistance (Curti and Faries, 2021), limited response to immunotherapy (Yu et al., 2019; Curti and Faries, 2021), and the occurrence of immune-related severe adverse events (Brahmer et al., 2018). The combination of immune modulators and targeted therapy showed encouraging results, and further studies are ongoing to address clinic exploitability (Ascierto et al., 2019; Dummer et al., 2022; Ferrucci et al., 2020; Gutzmer et al., 2020).

Given this scenario, new preclinical assays are required to identify druggable vulnerabilities and to design alternative treatments, focusing in particular on patients with limited therapeutic options (Garcia-Alvarez et al., 2021; Jenkins and Fisher, 2021; Moreira et al., 2021). In this study, we report the establishment of a fast and reliable preclinical model based on the migratory capacities of patient-derived cells to uncover melanoma sensitivities to targeted therapy. Indeed, migration signatures are reported to to predict patient survival (Nair et al., 2019), and we have previously shown that silencing of genes essential for in vivo melanoma growth concordantly reduced ex vivo cell migration (Bossi et al., 2016). We screened our melanoma patient-derived xenografts (PDXs) with a short hairpin RNA (shRNA) library of actionable genes and unveiled *AURKA* as essential for melanoma progression. We proved that the combination of

[1]*Department of Experimental Oncology, European Institute of Oncology, Istituto di Ricovero e Cura a Carattere Scientifico (IRCCS), Milan, Italy;* [2]*Fondazione Policlinico Universitario Agostino Gemelli, Istituto di Ricovero e Cura a Carattere Scientifico (IRCCS), Rome, Italy;* [3]*Unità Operativa Multizonale di Anatomia Patologica, Azienda Provinciale per i Servizi Sanitari, Trento, Italy;* [4]*CISMED - Centre for Medical Sciences, University of Trento, Trento, Italy;* [5]*Department of Oncology and Hemato-Oncology, University of Milan, Milan, Italy; and* [6]*Institute of Oncology Research, Oncology Institute of Southern Switzerland, Bellinzona, Switzerland*

Correspondence: Luisa Lanfrancone, Department of Experimental Oncology, European Institute of Oncology, Via Adamello 16 – 20139 Milan, Italy. E-mail: luisa.lanfrancone@ieo.it

Abbreviations: ATE, etomoxir with alisertib and trametinib; BC, barcode; CTR, control; DT, dabrafenib and trametinib; DEG, differentially expressed gene; Eto, etomoxir; FA, fatty acid; FAO, fatty acid oxidation; MEK, MAPK/extracellular signal–regulated kinase kinase; PDX, patient-derived xenograft; shRNA, short hairpin RNA

Received 8 July 2022; revised 2 February 2023; accepted 3 March 2023; accepted manuscript published online XXX; corrected proof published online XXX

alisertib (an AURKA inhibitor) with trametinib (a MAPK/extracellular signal–regulated kinase kinase [MEK] inhibitor, approved for melanoma treatment) additively inhibited ex vivo cell migration and in vivo growth of melanoma PDXs from different genetic backgrounds (*BRAF*/*NRAS*-mutant and triple wild type). We showed that alisertib and trametinib combination treatment induced upregulation of fatty acid oxidation (FAO) signaling, unveiling an acquired additional pharmacological vulnerability. The triple combination of alisertib, trametinib, and etomoxir (Eto), an inhibitor of the FAO pathway, clearly showed increased benefit, inducing tumor regression in vivo and prolonging the overall survival of the mice.

RESULTS

Ex vivo migration genetic screens identify multiple melanoma actionable vulnerabilities

We set up an alternative preclinical platform, exploiting the migratory features of our stages III–IV melanoma PDXs (Bossi et al., 2016). In particular, we focused on *BRAF*-mutant, *NRAS*-mutant, and triple wild type PDXs obtained from treatment-naïve patients that showed a poor overall response to treatments, suggesting intrinsic resistance (Supplementary Figure S1a). We characterized the migratory capacities of two metastatic melanoma PDXs—MM13 (NRAS-Q61L) and MM27 (BRAF-V600E)—by seeding cells in transwells and separately collecting migrated and non-migrated cells. PDXs showed a patient-specific migration rate at 24 hours (28% MM13 and 35% MM27), which was essentially unmodified at 48 hours (Supplementary Figure S1b). Conversely, proliferation did not change at 24 hours but was considerably raised at 48 hours (Supplementary Figure S1c) in both PDXs. To avoid any putative contribution of cell proliferation during the migration assay, we carried out the experiments for 24 hours.

To test the feasibility of a transwell-based ex vivo migration drop-out screen, MM13 and MM27 cells were transduced with a non targeting library composed of 1,200 molecular barcodes (BCs) vectors (Figure 1a). In both PDXs, the entire repertoire of BCs was recovered in the migrated and non-migrated cell populations, without appreciable differences in their distribution (nine and five differentially distributed BCs in MM13 and MM27, respectively) (Figure 1b).

We then performed the ex vivo migration screen with an shRNA library targeting 77 actionable genes (actionable library) (Figure 1a and Supplementary Figure S1d) that belong to many pathways frequently altered in cancer and that are targeted by already available drugs and could be potentially repurposed for melanoma treatment. PDX cells were transduced as described earlier, and migrated and non-migrated cells recovered after 24 hours. Notably, in both PDXs, the BC distributions of the actionable library were markedly shifted with respect to the corresponding non targeting ones (Figure 1b), highlighting numerous differentially distributed BCs between the two populations (134 BCs and 158 BCs in MM13 and MM27, respectively) (Figure 1b). To identify the actionable genes essential for melanoma migration, we scored shRNA depletion using an approach that combines two analyses on the basis of changes in BC frequencies in the migrated and non-migrated cell populations. Shift analysis identified genes with a global depletion drift among all targeting shRNAs (tier 1 genes) (Figure 1c, left panel), and combined significance analysis determined genes for which a significant number of highly depleted shRNAs were detected (tier 2 genes) (Figure 1c, right panel). By applying these two criteria, we identified 14 and 15 genes for MM13 and MM27, respectively, some of which have been previously associated with melanoma migration (phosphoinositide 3-kinase gene *PI3K*/protein kinase B gene *AKT*, *EGFR*, and *MDM2*) (Ma et al., 2020; Simiczyjew et al., 2019; Worrall et al., 2017). Most importantly, our screen identified several actionable candidates whose roles in migration were described in other solid cancers (*HSP90*, *PIP5K1A*, and *NTRK1*) (de la Mare et al., 2017; Sarwar et al., 2019; Yang et al., 2019), suggesting their role as therapeutic targets for drug repurposing in melanoma (Figure 1d).

Interestingly, only three identified hits were common between the two PDXs (AURKA, CCND1, and MDM2) (Figure 1e), delineating a highly patient-specific subset of essential genes.

Actionable ex vivo migration screens predict drug efficacy and define translationally relevant druggable profiles

To design alternative therapeutic strategies in melanoma, we focused on *AURKA* and *CCND1* (Figure 1d and e), whose inhibition had already been successfully tested in the clinic. Both genes are frequently overexpressed in human cancers, and their expression positively correlates with patient prognosis (González-Ruiz et al., 2020; Pathria et al., 2016; Puig-Butille et al., 2017; Xie and Meyskens, 2013). Besides regulating cell division, AURKA controls (CTRs) cell migration and adhesion, and its downregulation decreases motility in ovarian cancer (Do et al., 2014), head and neck squamous cell carcinoma (Wu et al., 2016), and melanoma (Xie and Meyskens, 2013). Cyclin D1 inhibition alters cell cycle progression and reduces cell movement in breast cancer (Dai et al., 2013; Qin et al., 2015) and sarcoma (Li et al., 2018).

AURKA and CCND1 expression was silenced in MM13 and MM27 PDXs using two pooled shRNAs, showing that each shRNA significantly downregulated target gene expression (Supplementary Figure S2a and b). In both PDXs, cell migration was strongly reduced upon *AURKA* or *CCND1* genetic silencing at 24 hours (Figure 2a). Notably, within this experimental timeframe, cell proliferation was not affected by gene depletion, either in the experimental conditions of the migration assay (Supplementary Figure S2c) or in a cell viability assay (Supplementary Figure S2d). To further corroborate this finding, we pretreated AURKA-/CCND1-silenced MM27 cells with the proliferation inhibitor mitomycin C and showed that migration rate was considerably inhibited (Supplementary Figure S2e) to levels comparable with those obtained in untreated cells. Of note, AURKA-targeted shRNA and CCND1-targeted shRNA cells did not undergo apoptosis in the corresponding experimental window (Supplementary Figure S2f).

To prove the efficacy of the underlying actionability approach, AURKA activity was specifically inhibited by alisertib (MLN8237), and CCND1 was indirectly targeted by palbociclib, a highly selective CDK4/6 inhibitor. Both drugs significantly reduced cell migration in MM13 and MM27,

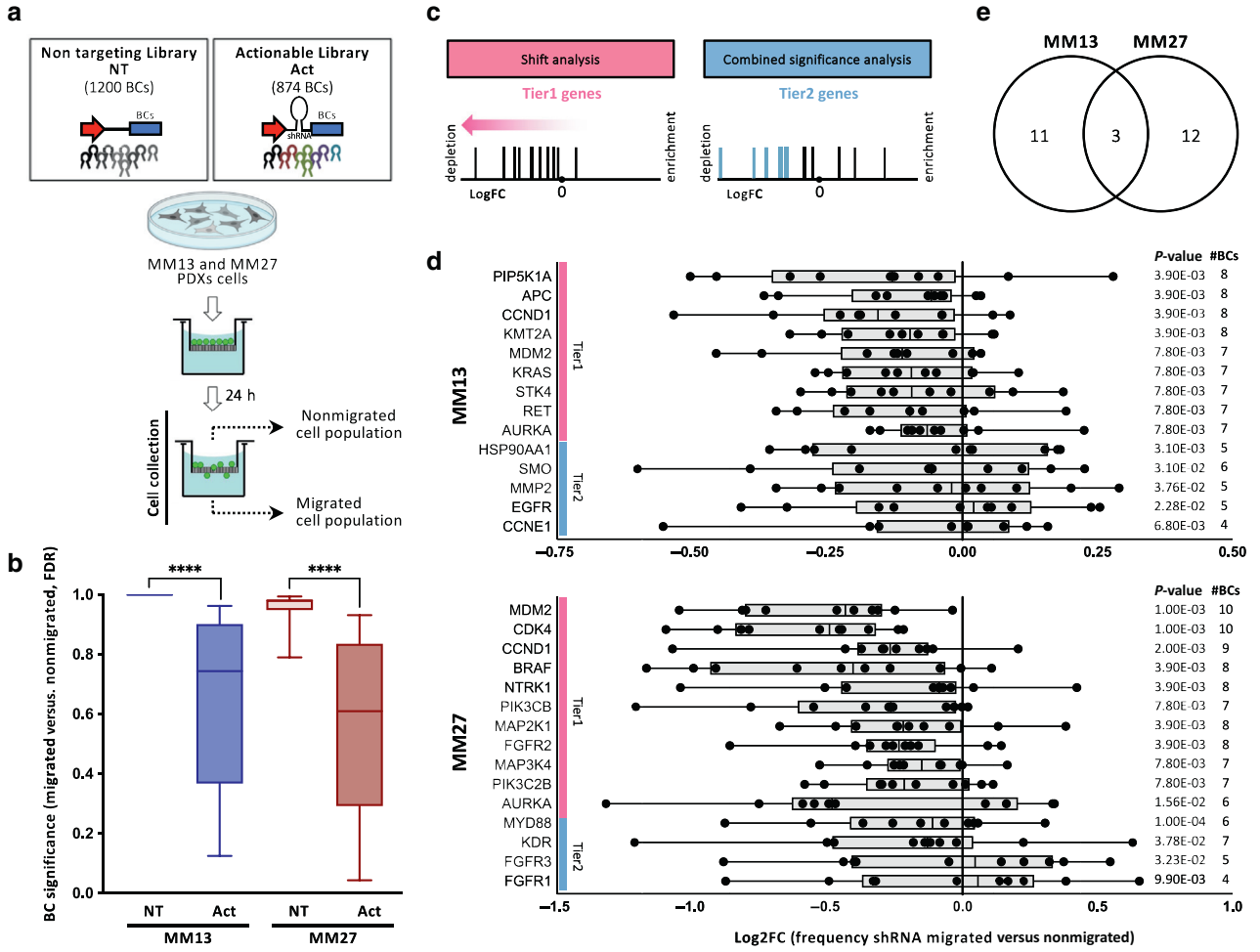

Figure 1. Ex vivo migration genetic drop-out screen is a feasible approach to unveil actionable vulnerabilities in melanoma PDXs. (**a**) Workflow of ex vivo transwell-based migration actionable genetic screen in MM13 and MM27 PDXs. (**b**) Barcoded-shRNA (BC) distribution between the migrated and non-migrated populations (FDR). The box line indicates the median; whiskers include 10–90 percentile data (****$P < 0.0001$ by an unpaired Mann–Whitney test). (**c**) Ex vivo migration screen analysis: a two-criteria analysis is integrated to define depleted genes in the migrated compartment. (**d**) MM13 and MM27 screen candidates essential for PDX migration. The distribution of log_2FC of shRNA-BCs frequencies (migrated vs. non-migrated population) is reported for each gene. Global *P*-value and the number of depleted BCs are indicated. (**e**) A Venn diagram of common and PDX-specific migration actionable candidates. Act denotes actionable, and NT denotes non targeting; BC, barcode; FC, fold change; FDR, false discovery rate; h, hour; MMP2, matrix metalloproteinase 2; PDX, patient-derived xenograft; shRNA, short hairpin RNA.

even at low doses, showing a dose-dependent effect (Figure 2b). These drugs may be considered two promising points of therapeutic intervention because alisertib already displayed good antitumor activity when administered in combination regimes in phase II and phase III clinical trials, including melanoma (Du et al., 2021), and palbociclib is a Food and Drug Administration–approved drug for the treatment of estrogen receptor–positive HER2-negative metastatic breast cancer, currently under evaluation in phase II clinical trials for melanoma (NCT03454919).

To investigate the translational potential of the isolated actionable candidates, we carried out in vivo drop-out screens in MM13/MM27 cells transduced with the actionable library and transplanted orthotopically in NOD scid gamma mice (Figure 2c). BC analyses revealed a full representation of the library in each tumor replicate, and BC frequencies were calculated as previously reported (Bossi et al., 2016). The BCs log_2 fold change distribution was shifted toward negative values, suggesting that gene silencing conferred an overall growth disadvantage to melanoma development in vivo (Supplementary Figure S2g). We scored 31 and 28 candidates for MM13 and MM27, respectively, one third of whom were common (Supplementary Figure S2h). On the basis of the identified hits in the ex vivo and in vivo screens, we performed pathway analyses to build PDX-specific vulnerability profiles. Strikingly, many pathways were essential in both the in vivo and ex vivo processes (Figure 2d), indicating that the ex vivo migration screen was able to predict vulnerabilities uncovered by the in vivo tumor growth screen, as anticipated earlier (Bossi et al., 2016). Interestingly, some pathways emerged as essential to sustain both MM13 and MM27 melanoma maintenance, and among them, AURKA signaling scored as the top ranking, proving to be essential in vivo (Figure 2d and Supplementary Figure S2i).

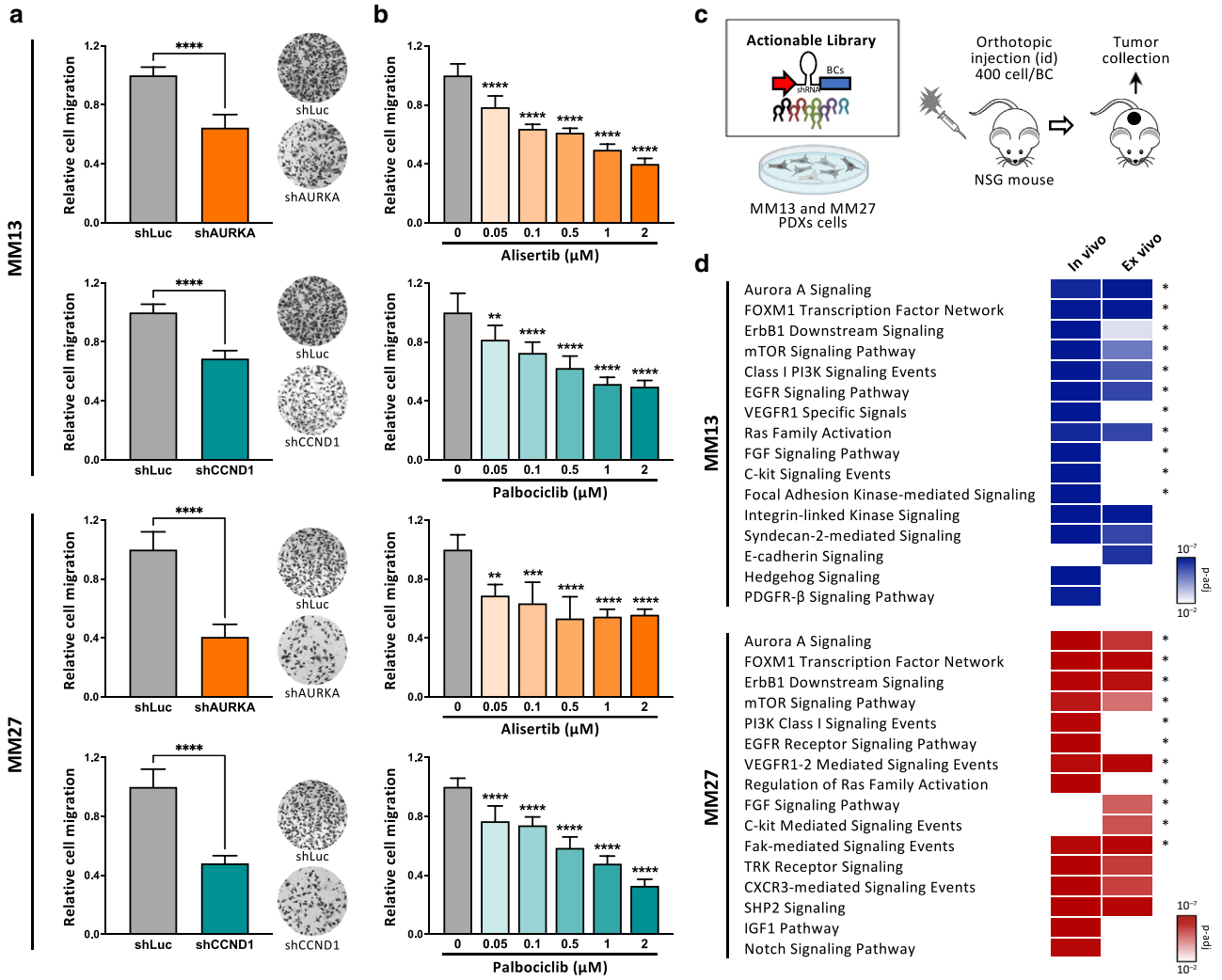

Figure 2. Actionable PDX profiles defined by ex vivo migration screen recapitulate in vivo vulnerabilities. (**a**) Effect of *AURKA* and *CCND1* gene silencing on MM13/MM27 PDX migratory capacities (values are normalized to shLuc; ***$P < 0.001$ and ****$P < 0.0001$ by unpaired *t*-test). Representative images of migrated cells (transwell outer surface) are reported. (**b**) Effect of alisertib (AURKA inhibitor) and palbociclib (CDK4/6 inhibitor) treatments on MM13/MM27 PDX migratory capacities (values are normalized to those of DMSO-treated samples; **$P < 0.01$, ***$P < 0.001$, and ****$P < 0.0001$ by unpaired *t*-test). (**c**) Workflow of in vivo tumor growth actionable genetic screening on MM13 and MM27. (**d**) Pathway analysis of MM13/MM27 in vivo and ex vivo candidates (combined score-based ranking index < 50, adjusted $P < 0.01$; EnrichR, National Cancer Institute Nature2016 Database). Common pathways in MM13 and MM27 are indicated with an asterisk (*). id, intradermal; NSG, NOD scid gamma; PDX, patient-derived xenograft; PI3K, phosphoinositide 3-kinase; shAURKA, AURKA-targeted short hairpin RNA; shCCND1, CCND1-targeted short hairpin RNA; shLuc, luciferase-short hairpin RNA.

Alisertib and trametinib combination is an effective alternative therapeutic approach in advanced and therapy-resistant melanomas

MEK inhibitors are approved for the treatment of patients with *BRAF*-mutant melanoma in combination with BRAF inhibitors (Long et al., 2017). Recently, MEK blockade has shown an acceptable safety profile and antitumor activity in non–*BRAF*-mutant melanomas (Garcia-Alvarez et al., 2021). Therefore, we decided to use alisertib in combination with trametinib to treat six metastatic PDXs with different genetic backgrounds (Supplementary Figure S1a). Both drugs significantly reduced cell migration when administered as single agents, and their combination showed a remarkable additive effect in all PDXs (50–80% migration rate reduction) (Figure 3a). To the best of our knowledge, this is previously unreported evidence of alisertib and trametinib combination efficacy in melanoma, independently from the harboring genetic background, which is particularly relevant for patients with non-*BRAF* mutations who still lack effective treatment opportunities.

In *BRAF*-mutant melanomas (MM27 and MM2), we compared the alisertib and trametinib combination with the standard-of-care therapy, that is, the dabrafenib and trametinib (DT) combination. MM27 and MM2 cells were treated with alisertib or dabrafenib (at doses that equally affected cell viability) (Supplementary Figure S3a) and trametinib. The alisertib and trametinib combination proved superior efficacy to DT combination in reducing the migration rate (24 and 45% increased efficacy in MM27 and MM2, respectively) (Figure 3b), suggesting that the alisertib and trametinib is a valid alternative combination treatment.

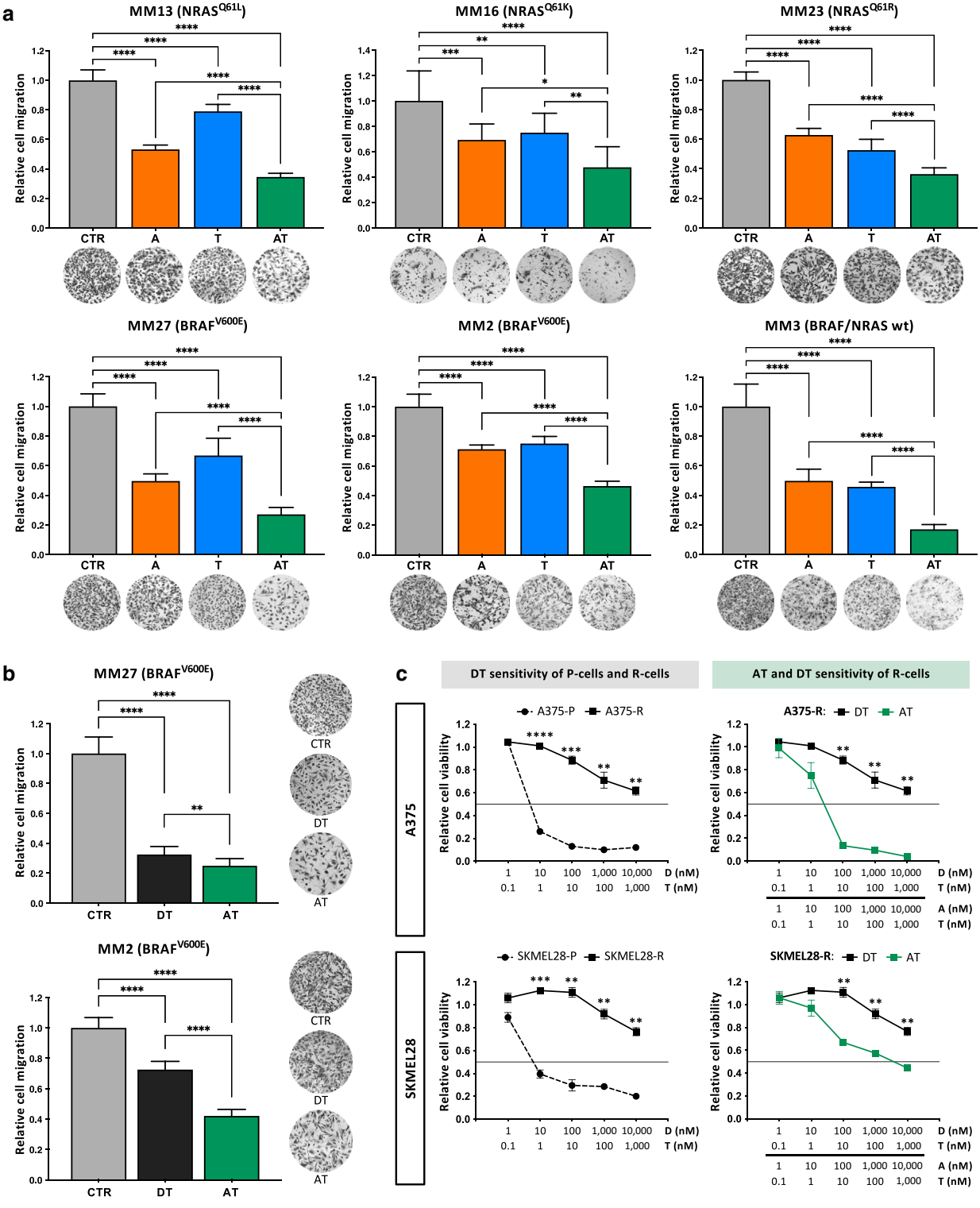

Figure 3. Alisertib and trametinib combination is an effective therapeutic approach in advanced melanomas, outperforms standard-of-care regimen, and overcomes therapy resistance. (**a**) Effect of alisertib and trametinib combination on six PDX migratory capacities (values are normalized to those of vehicle-treated samples, CTR; $*P < 0.05$, $**P < 0.01$, $***P < 0.001$, and $****P < 0.0001$ by one-way ANOVA). Representative images of migrated cells are reported. (**b**) Effect of AT and dabrafenib and trametinib combinations on MM27/MM2 *BRAF*-mutant PDXs (values are normalized to those of the CTR; $**P < 0.01$ and $****P < 0.0001$ by unpaired *t*-test). Representative images of migrated cells are reported. (**c**) A375 and SKMEL28 parental (P-cells) and resistant (R-cells) cell lines' sensitivity to DT (left). Resistant cell lines (A375-R, SKMEL28-R) sensitivity to AT and DT (right) (CyQuant assay; values are normalized to those of the corresponding CTR; $**P < 0.01$, $***P < 0.001$, and $****P < 0.0001$ by unpaired *t*-test). A denotes alisertib, T denotes trametinib, AT denotes alisertib and trametinib combination, D denotes dabrafenib, and DT denotes dabrafenib and trametinib combination. CTR, control; PDX, patient-derived xenograft; wt, wild type.

Furthermore, we tested the alisertib and trametinib combination in drug-resistant A375 and SKMEL28 *BRAF*-mutant melanoma cell lines (R-cells, A375-R, and SKMEL28-R) (Caporali et al., 2017, 2016). They showed reduced sensitivity to DT combination compared with their parental counterparts (P-cells, A375-P, and SKMEL28-P) (Figure 3c, left, and Supplementary Figure S3b). In R-cell, alisertib and trametinib treatment proved to be extremely effective (Figure 3c, right), suggesting that the newly proposed regimen may be beneficial in drug-resistant or relapsing patients.

Alisertib and trametinib combination severely reduces in vivo tumor growth

We then assessed alisertib and trametinib combination activity in vivo in NOD scid gamma mice orthotopically injected with MM13 and MM27 cells. When tumors reached ~70–80 mm^3 volumes, mice were randomized to receive vehicle (CTR), alisertib, trametinib, or their combination. All treatments were very well-tolerated in vivo, with no significant body weight loss in mice during the therapeutic window (Supplementary Figure S4a). Drug vehicles proved to be safe because untreated and vehicle-treated mice did not show any adverse effects (Supplementary Figure S4b–d). In both PDXs, alisertib or trametinib alone significantly reduced tumor growth rate, whereas the combination showed an additive inhibition of tumor growth (89 and 68% tumor volume reduction in MM13 and MM27, respectively, compared with CTR treatment) (Figure 4a and b and Supplementary Figure S4e), validating the predictive value of our ex vivo migration screen. Notably, in both PDXs, we observed partial tumor regressions at the end of the treatment (17% at one of six and 9% at 1 of 11 for MM13 and MM27, respectively). Moreover, the alisertib and trametinib combination prolonged mouse survival with an increased median life span of 33 and 42% with respect to vehicle-treated mice in MM13 and MM27, respectively (Figure 4c).

Histological analyses revealed that both drugs exerted an on-target effect by reducing AURKA and MAPK phosphorylation (Supplementary Figure S4f). Furthermore, vehicle- and single-drug–treated tumors displayed a dense cellular architecture, whereas alisertib and trametinib combination–treated ones exhibited decreased cellularity because of the substitution of tumor parenchyma with hyaline connective tissue as a reparative outcome after tumor necrosis in both PDXs. Alisertib and trametinib treatment induced a dramatic inhibition of cell proliferation (reduction of Ki-67+ cells) and, inversely, an increased cell cycle blockade (increment of p21+ cells) (Figure 4d).

Alisertib and trametinib combination downregulates numerous critical cancer pathways

To investigate the mechanism through which the alisertib and trametinib combination leads to tumor reduction, we evaluated its effect on cell cycle regulation in MM13 and MM27 PDXs. We showed a robust G2/M phase arrest after treatment with alisertib (40% increase of G2 cells in MM13 and 52% in MM27) and a remarkable G1 phase delay upon trametinib administration (22% increase of G1 cells in MM13 and 44% in MM27 cells). Alisertib and trametinib treatment induced an intermediate arrest in both G1 and G2/M phases, with a strong additive reduction of S phase (from 23 to 1% in MM13 and from 43 to 3% in MM27), as previously reported in colon cancer cell lines (Davis et al., 2015) (Figure 5a and Supplementary Figure S5a).

To shed light on the pathways mediating the additive effect of the alisertib and trametinib combination, we analyzed early transcriptional regulation in MM27-treated cells by bulk RNA sequencing. Two-dimensional principal component analysis revealed a clear segregation of transcriptional profiles, with alisertib and trametinib combination–treated cells displaying the widest divergence than both CTRs and monotherapies (Figure 5b). Subsequently, we examined differentially expressed genes (DEGs) upon treatment (each treatment compared with DMSO-treated cells). Monotherapies induced the regulation of distinct, small, nonoverlapping sets of genes (20 DEGs for alisertib and 347 DEGs for trametinib), whereas alisertib and trametinib treatment elicited the highest degree of transcriptional regulation (2,653 DEGs) and the greatest percentage of uniquely identified DEGs (86.2%), including almost all the DEGs induced by the two monotherapies (Figure 5c). Notably, common DEGs in monotherapies and combination treatment showed a marked regulation in the latter (both down and upregulated) (Supplementary Figure S5b). Gene ontology analysis showed that alisertib induced the downregulation of many cell cycle–related functions (DNA replication, G2/M transition); trametinib negatively modulated cell proliferation (G1/S transition) and MAPK pathways; and the combination strongly attenuated transcription, proliferation, migration, cell adhesion, and early apoptotic processes (Supplementary Figure S5c).

Pathway analysis of downregulated genes (Ingenuity Pathway Analysis) revealed an attenuation of critical cancer pathways upon alisertib and trametinib combination administration (Gene Set Enrichment Analysis, Kyoto Encyclopedia of Genes and Genomes database) (Supplementary Figure S5d). In particular, the epithelial–mesenchymal transition process and many GF-mediated signaling pathways (PDGF, fibroblast GF, VEGF, ILK, and Hippo) proved to be involved in alisertib and trametinib combination–mediated regulation, but overall, they were similarly affected by the two monotherapies (Supplementary Figure S5e). Conversely, pathways underpinning motility and IGF-1, HGF, ILs, CXCR4, AMPK, Wnt/β-catenin, and mTOR signaling cascades showed stronger inhibition upon alisertib and trametinib combination than on monotherapies (additive score of more than 100-fold increase in fold change) (Figure 5d).

We then combined the two lists of alisertib and trametinib monotherapies DEGs into a merged list (alisertib union trametinib, i.e., AUT), which represents the predicted transcriptomic regulation exerted by the union of the biological effects of the two single treatments (as reported for biological process analysis [Diaz et al., 2020]). Interestingly, we showed that the majority of genes are uniquely regulated in the alisertib and trametinib condition because only 34% of the downregulated genes overlap between alisertib and trametinib (experimental combination) and AUT (predicted combination) (Supplementary Figure S5f). Moreover, the alisertib and trametinib and AUT common downregulated genes showed significantly lower log_2fold change value distribution in alisertib and trametinib than in AUT (Figure 5e). The two conditions showed strikingly different patterns of pathway

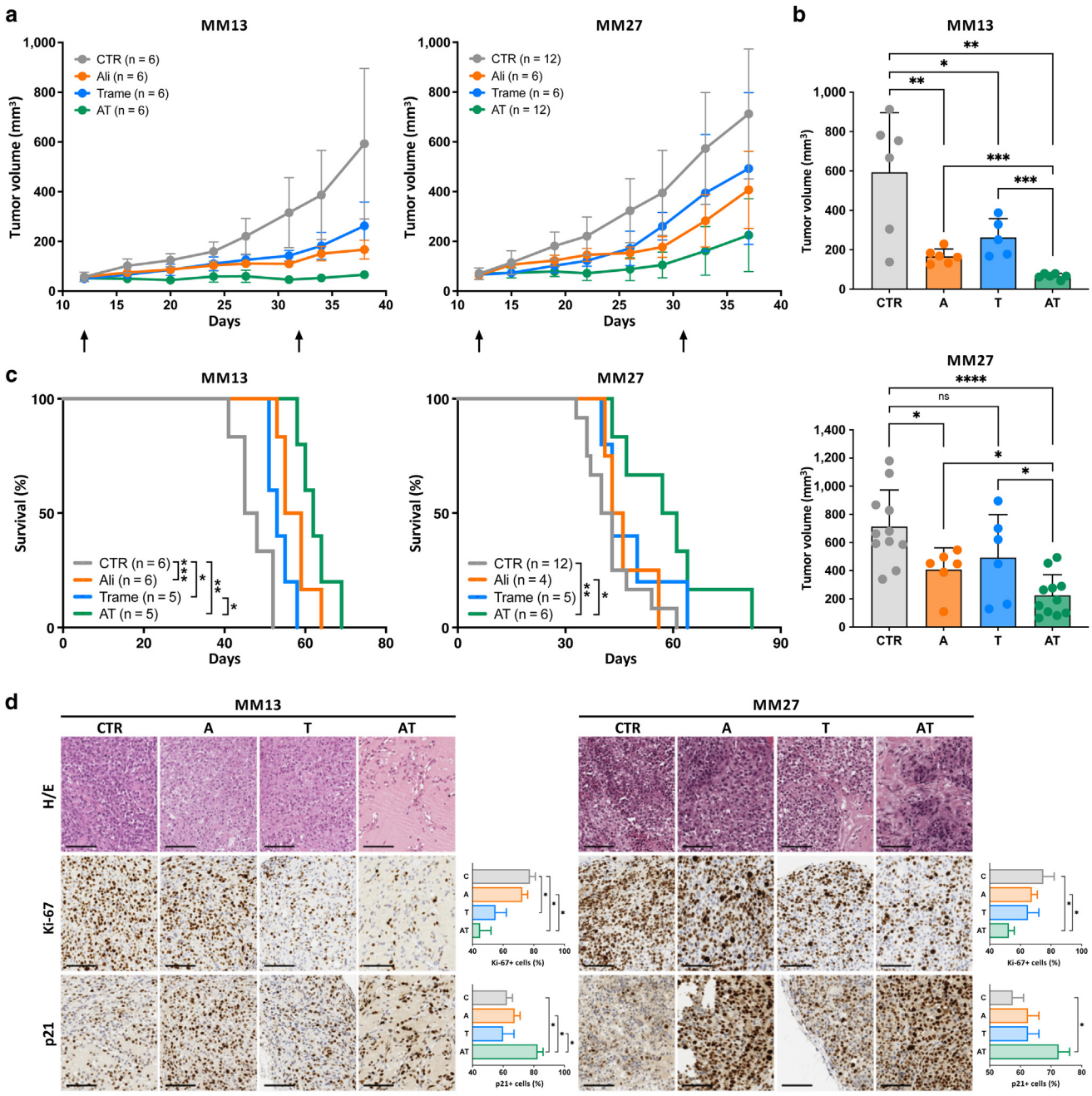

Figure 4. Alisertib and trametinib combination additively reduce in vivo tumor growth and prolongs mice survival in MM13 and MM27 PDXs. Assessment of AT activity in vivo in MM13 and MM27 (vehicle, CTR; alisertib, 20 mg/kg; trametinib, 0.5 mg/kg; po qd × 5 ×3w). (**a**) Tumor growth curves (black arrows indicate treatment administration window). (**b**) Tumor volumes quantification (6 days after last treatment; $^{*}P < 0.05$, $^{**}P < 0.01$, $^{***}P < 0.001$, and $^{****}P < 0.0001$ by unpaired *t*-test). (**c**) Survival analysis by Kaplan–Meier curves ($^{*}P < 0.05$, $^{**}P < 0.01$, and $^{***}P < 0.001$ by log-rank Mantel–Cox test). (**d**) Immunohistochemistry analysis of MM13/MM27 AT-treated tumors. Representative images and quantification of Ki-67 and p21 are reported (bar = 100 μm; $^{*}P < 0.05$ by unpaired *t*-test). A denotes alisertib, T denotes trametinib, AT denotes alisertib and trametinib combination, Ali denotes alisertib, and Trame denotes trametinib. CTR, control; ns, not significant; PDX, patient-derived xenograft; po qd × 5 ×3w, per os quaque die (once a day) for 5 days for 3 weeks.

regulation, suggesting that the alisertib and trametinib combination exceeds the bare sum of the effects of the two monotherapies (Figure 5d and Supplementary Figure S5e).

The mTOR pathway emerged as highly downregulated upon alisertib and trametinib combination at the transcriptional level (Figure 5d) and, concordantly, also the mTORC1 and mTORC2 effector complexes (Figure 5f). Protein expression of total and phosphorylated mTOR, p70-S6K, S6, and eIF2α was used to assess the activation status of the mTOR signaling pathway, showing its reduced activation in MM27 and also in MM13 PDX cells upon alisertib and trametinib treatment (Figure 5g). Notably, mTOR emerged as a vulnerable pathway in both PDXs in our ex vivo and in vivo screens (Figure 2d), and increased activation of the protein kinase B/mTOR pathway is reported in around 70% of metastatic melanomas (Chamcheu et al., 2019), thus suggesting

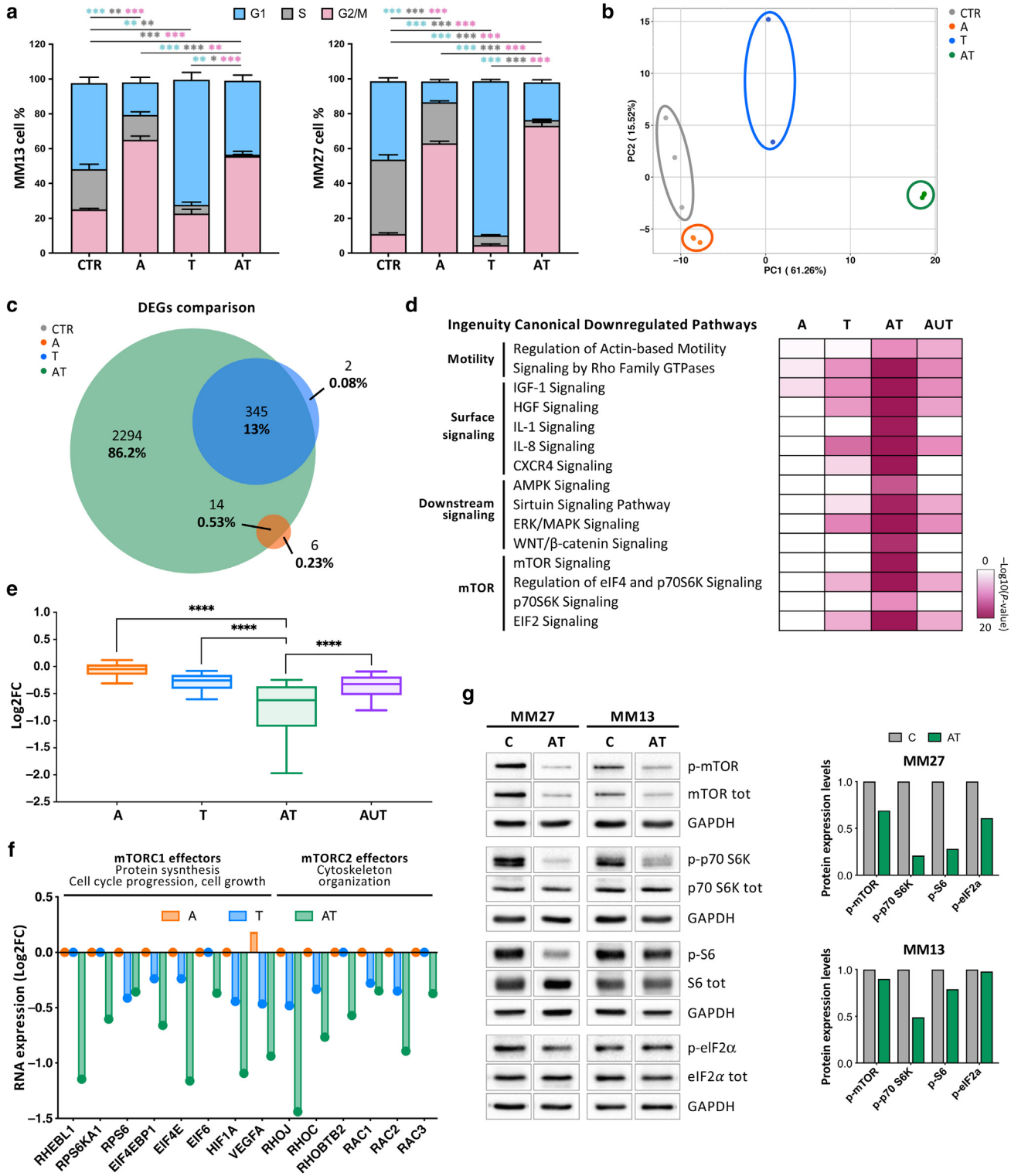

Figure 5. Alisertib and trametinib combination regulate cell cycle and transcriptomic profiles, leading to the downmodulation of numerous critical cancer pathways. (**a**) Cell cycle analysis (BrdU PI) of AT-treated MM13/MM27 cells. The bar graph shows the percentage of cells in G1, S, and G2/M phases (*$P < 0.05$, **$P < 0.01$, and ***$P < 0.001$ by unpaired *t*-test). (**b**–**f**) Transcriptomic regulation (bulk RNAseq) of MM27 A-, T-, and AT-treated cells. Two-dimension PCA. (**b**) Venn diagram of DEGs for each treatment (compared with that of vehicle-treated sample, CTR; $|\log_2 FC| > 1$ and adjusted $P < 0.05$). (**c**) Heat map of downmodulated pathways (Ingenuity Pathway Analysis; adjusted $P < 0.05$; AS > 2; AUT as merged list of DEGs of A and T). (**d**) Log_2FC distribution of downregulated genes is shown; the box line indicates the median, and whiskers include 10–90 percentile data (****$P < 0.0001$ by unpaired Mann–Whitney test). (**e, f**) Transcriptional regulation of mTORC1 and mTORC2 downstream elements. (**g**) The protein expression level of mTOR pathway downstream targets upon AT treatment in MM27 and MM13 cells. Representative western blots and densitometry analysis are reported. A denotes alisertib, T denotes trametinib, AT denotes alisertib and trametinib combination, and AuT denotes alisertib union trametinib. AS, additive score; CTR, control; DEG, differentially expressed gene; FC, fold change; PCA, principal component analysis; p-eIF2α, phosphorylated eIF2α; PI, propidium iodide; p-mTOR, phosphorylated mTOR; p-p70 S6K, phosphorylated p70 S6K; p-S6, phosphorylated S6; RNAseq, RNA sequencing.

that the alisertib and trametinib combination inhibits a crucial pathway for melanoma maintenance.

Alisertib and trametinib treatment induces upregulation of FAO, unveiling an acquired pharmacological vulnerability

We next focused on transcriptionally upregulated pathways in MM27 alisertib and trametinib combination–treated cells, showing significant enrichment of fatty acid (FA) beta-oxidation (i.e., FAO) and oxidative phosphorylation pathways (Gene Set Enrichment Analysis, Gene Ontology Biological Process, and Kyoto Encyclopedia of Genes and Genomes datasets) (Figure 6a). In particular, we annotated upregulated genes involved in several steps of the FA catabolic process: FA transport, Acyl-CoA synthesis, carnitine-mediated transport across the mitochondria membrane, and beta-oxidation (Figure 6b). We then assessed transcriptional modulation of a subset of genes regulating different steps of FAO (*BBOX1*, *FABP3*, *FA2H*, *ACADS*, and *ACSM5*) and showed that they were upregulated in MM27 and also in MM13 alisertib and trametinib combination–treated cells (Figure 6c). These observations support the evidence that exposure to therapies reprograms *BRAF*-mutant melanoma cell metabolism toward increased FA catabolism (Aloia et al., 2019; Rambow et al., 2018; Shen et al., 2020), extending this mechanism to *NRAS*-mutant melanomas. Given that this metabolic shift also defines a trait of drug-tolerant persister cells, possibly founders of acquired resistance (Alkaraki et al., 2021), we analyzed MM27 alisertib and trametinib combination–treated tumors that relapsed after treatment discontinuation (denoted as AT-tum) (Figure 4 and Supplementary Figure S6a). Cells derived from these tumors showed reduced sensitivity to alisertib and trametinib ex vivo (Figure 6d) and a remarkable transcriptional upregulation of FAO genes compared with those from CTR tumors (denoted as CTR-tum) (Figure 6e). Therefore, we pharmacologically targeted the FAO pathway using Eto, an irreversible inhibitor of the carnitine palmitoyltransferase CPT1 enzyme. AT-tum cells were remarkably more sensitive to Eto than CTR-tum cells (Figure 6f and Supplementary Figure S6b), suggesting that alisertib and trametinib combination treatment unveils an acquired pharmacological vulnerability that is efficiently targeted by Eto.

We postulated that the concomitant administration of Eto with alisertib and trametinib (ATE) may be the most effective strategy. Indeed, the ATE triple combination further reduced cell migration in both MM27 and MM13 cells compared with alisertib and trametinib combination treatment (Figure 6g and Supplementary Figure S6c). Interestingly, although treatment with Eto alone reduced migration by 28% (MM27) and 20% (MM13) (Eto vs. CTR), the migration rate dropped by 40% (MM27) and 56% (MM13) when Eto was added to alisertib and trametinib treatment (ATE vs. alisertib and trametinib). Moreover, ATE coadministration was able to significantly reduce alisertib and trametinib combination–induced FAO transcriptional expression, indicating that the addition of Eto partially rescued FAO upregulation (Figure 6h and Supplementary Figure S6d).

Then, we tested the ATE triple combination in vivo by simultaneous administration of the three drugs in MM27 PDX (Supplementary Figure S6e and f), showing that the triple combination was well-tolerated (Supplementary Figure S6e). Eto alone did not show any efficacy in controlling tumor growth, whereas the ATE triple combination was extremely effective, reducing tumor growth by 93% compared with CTR and strikingly by 77% with respect to the alisertib and trametinib dual combination (Figure 6i and j and Supplementary Figure S6f). In particular, the ATE treatment was able to induce partial tumor regression in >70% of mice at the end of the treatment schedule (Figure 6j and k and Supplementary Figure S6f). ATE triple combination significantly prolonged mice overall survival, extending median overall survival by 128.9% (53.5 days) compared with CTR and notably by 61% (36 days) compared with alisertib and trametinib group (Figure 6l and Supplementary Figure S6f), suggesting a potential clinical efficacy of the ATE triple combination.

Discussion

Despite remarkable advances in melanoma clinical management, the high rate of recurrences, mainly because of the development of primary or acquired resistances, limits their application, making alternative therapeutic strategies highly required for advanced and metastatic patients (Jenkins and Fisher, 2021). The development of more informative preclinical assays and the identification of relevant tumor vulnerabilities are needed to support preclinical research and to design and test alternative, effective therapeutic options for patients with melanoma.

To build a reliable preclinical assay, we made use of our cohort of metastatic melanoma PDXs, which recapitulate the genetic and functional heterogeneity of the corresponding tumor of origin (Bossi et al., 2016). To functionally characterize actionable vulnerabilities and obtain translationally predictive results (Bossi et al., 2016; Nair et al., 2019), we conducted ex vivo genetic screens, assessing the cell migration capabilities of our PDX cells. We used an ad hoc–designed shRNA library of actionable genes associated with available drugs to envision a rapid repositioning for melanoma. To this end, the shRNA-mediated gene silencing approach is preferable to genetic ablation because it closely mirrors the activity of pharmacologic inhibitors. In this study, we report the evidence of a drop-out ex vivo migration genetic screen carried out in melanoma, never previously performed in this tumor type. Of note, many migration genetic screens have been performed in other tumor models, mainly in cell lines (Caino et al., 2016; Koedoot et al., 2019; Rossi et al., 2021; Su et al., 2014; Tajadura-Ortega et al., 2018; van Roosmalen et al., 2015; Yang et al., 2013), with the aim of isolating migration suppressor genes which are difficult to be used as a point of therapeutic intervention (Caino et al., 2016; Su et al., 2014; Yang et al., 2013). Conversely, we performed ex vivo migration drop-out screens in patient-derived models, identified drug repurposing candidates, and showed that they are also essential for tumor growth in vivo, thus defining a previously unreported useful preclinical tool. Then, on the basis of functional data from our screens, we built PDX-specific profiles of vulnerable pathways, showing that MM13 and MM27 were characterized by

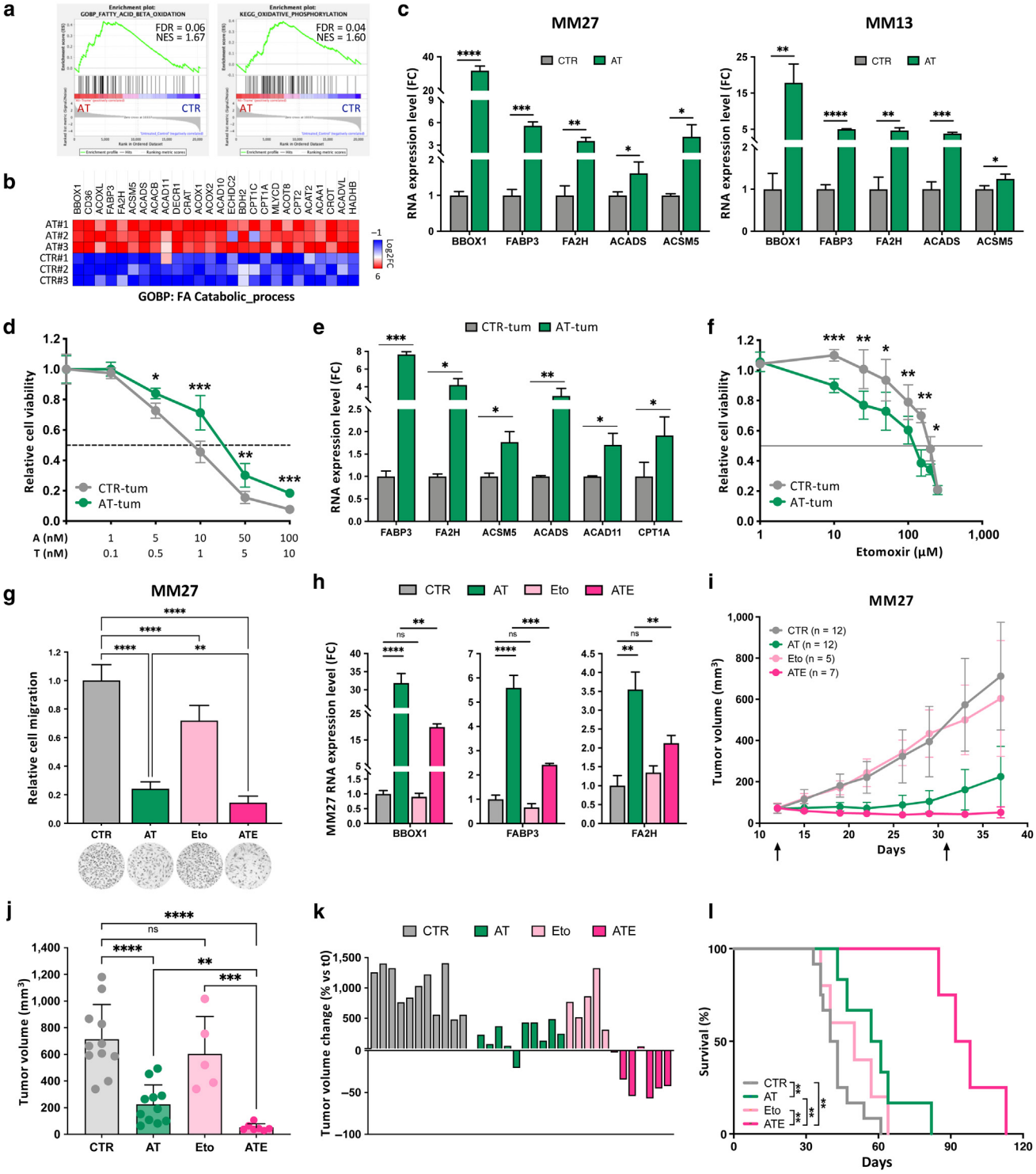

Figure 6. Targeting upregulated FAO pathway in AT-treated cells and relapsing tumors promotes cancer regression and mice survival. (**a, b**) Analysis of transcriptionally upregulated genes in MM27 AT-treated cells (compared with those in the CTR). (**a**) GSEA profiles (adjusted $P < 0.05$) and (**b**) heat map (Morpheus designing tool; https://software.broadinstitute.org/morpheus). (**c**) Transcriptional expression levels of FAO genes in MM27/MM13 AT-treated cells (normalized to those of DMSO-treated samples, CTR; ***$P < 0.001$ and ****$P < 0.0001$ by unpaired *t*-test). (**d**) Ex vivo AT sensitivity of in vivo AT-treated tumor-derived cells (AT-tum; compared with that of control-treated tumors, CTR-tum; *$P < 0.05$, **$P < 0.01$, and ***$P < 0.001$ by unpaired *t*-test). (**e**) Transcriptional expression levels of FAO genes in CTR-tum/AT-tum cells (*$P < 0.05$, **$P < 0.01$, and ***$P < 0.001$ by unpaired *t*-test). (**f**) CTR-tum/AT-tum cells ex vivo sensitivity to etomoxir (FAO inhibitor, Eto) (*$P < 0.05$, **$P < 0.01$, and ***$P < 0.001$ by unpaired *t*-test). (**g**) Effect of ATE simultaneous treatment on MM27 migratory capacities (**$P < 0.01$, ***$P < 0.001$, and ****$P < 0.0001$ by one-way ANOVA). (**h**) Transcriptional expression levels of FAO genes upon ATE treatment in MM27 (*$P < 0.05$, **$P < 0.01$, and ***$P < 0.001$ by unpaired *t*-test). (**i−l**) Assessment of ATE activity in vivo in MM27 tumor growth curves (vehicle, CTR; Eto, 20 mg/kg; AT, 20 mg/kg for alisertib + 0.5 mg/kg for trametinib; ATE, 20 mg/kg for alisertib + 0.5 mg/kg for trametinib + 20 mg/kg for Eto; po qd × 5 × 3w) (black arrows indicate treatment administration window). (**i**) Tumor volumes quantification (6 days after last treatment; **$P < 0.01$, ***$P < 0.001$, and ****$P < 0.0001$ by unpaired *t*-test). (**j**) Single tumor volume change percentage (6 days after last treatment compared with that at t0, treatment start). (**k, l**)

some common signaling (AURKA, ErbB1, EGFR, mTOR/phosphoinositide 3-kinase, VEGFR, and fibroblast GF signaling pathways) as well as patient-specific dependencies (integrin, E-cadherin signaling in MM13; TRK, IGF-1, and the Notch pathway in MM27). Our approach successfully captured actionable relevant dependencies in melanoma because the inhibition of many identified genes already showed preliminary antitumor activity when tested in clinical trials, especially in combination regimens (NCT01820364, NCT03611868, NCT02097225, NCT04356729, and NCT00909831).

We focused on AURKA, targeting it with alisertib in combination with trametinib and proving that their combination is crucial to improving therapeutic potency for the treatment of metastatic melanoma. In the preclinical setting, this combination was reported to be effective in controlling tumor growth rate in restricted subtypes of colon (Davis et al., 2015), pancreatic, and lung (Vallejo et al., 2017) carcinomas, but its mechanism of action has not been dissected yet. In melanoma, AURKA and BRAF/MAPK pathway targeting was described as an efficient therapeutic strategy in vitro because combinations of AURKA, BRAF, and/or MEK inhibitors showed antiproliferative activity (Caputo et al., 2014; Margue et al., 2019; Pathria et al., 2016). In this study, we proved that the alisertib and trametinib combination is highly effective, outperforming the effect of standard-of-care therapy in our *BRAF*-mutant melanoma PDXs and showing effectiveness in melanoma models of acquired resistance. When coadministered in vivo, alisertib and trametinib showed an optimal safety profile and an additive effect in controlling tumor growth, with a significant reduction of Ki-67+ proliferating cells. Indeed, alisertib and trametinib combination induced a prominent cell cycle arrest by double blockade of the G1 and G2/M phases and a strong reduction of the S phase, as previously reported in colon cancer (Davis et al., 2015).

Alisertib and other AURKA inhibitors showed encouraging clinical activity with a manageable safety profile in clinical trials for a broad range of tumors, including melanoma (NCT01045421, NCT01653028, NCT01799278, NCT01466881, and NCT01316692 [Du et al., 2021]), and in many combination schedules (NCT01094288, NCT01091428, NCT01639911, NCT01567709, and NCT04085315 [Du et al., 2021]). Trametinib is an already Food and Drug Administration–approved drug for the treatment of *BRAF*-mutant melanomas, and MEK inhibition showed favorable efficacy also for non–*BRAF*-mutant melanoma subtypes in several clinical trials in combination with targeted agents (NCT01781572, NCT03947385, NCT02110355, and NCT01985191 [Curti and Faries, 2021; de Weger et al., 2019; Schuler et al., 2022; Tolcher et al., 2018]). Thus, the alisertib and trametinib combination may represent a valid alternative therapeutic approach for melanoma.

Moreover, we provide a supporting mechanism for alisertib and trametinib combination that was not previously dissected, proving that its additive effect partly resides at the transcriptional level. Indeed, alisertib and trametinib combination–treated cells displayed a higher level of transcriptional rewiring than monotherapy, with many motility and proliferation pathways exclusively inhibited in the combination-treated cells. Thus, the alisertib and trametinib effect is possibly sustained by the orchestrated reduction of the activity of many oncogenic pathways, among which mTOR appears to be crucial because its activation has been extensively associated with melanoma pathogenesis (Chamcheu et al., 2019) and has also been confirmed as a vulnerable pathway in our screen.

Exposure to targeted therapies, mainly BRAF and MEK inhibitors, is known to induce metabolic reprogramming toward enriched FA transport and mitochondrial/peroxisomal lipid catabolism (Aloia et al., 2019; Rambow et al., 2018; Shen et al., 2020), as also confirmed in patient cohort analyses (Aloia et al., 2019; Shen et al., 2020; Zhang et al., 2016). Interestingly, we corroborated these data, scoring a marked transcriptional upregulation of genes involved in lipid catabolism in both PDXs upon alisertib and trametinib treatment. We highlighted increased FAO expression also in relapsing tumors after alisertib and trametinib treatment discontinuation, thus suggesting a leading role for this pathway in sustaining relapse. Taking advantage of this acquired therapeutic vulnerability, we showed that cells derived from alisertib and trametinib combination–treated, relapsed PDX tumors (AT-tum cells) were extremely sensitive to the FAO inhibitor Eto.

Eto alone was barely effective in PDX cells, whereas it remarkably reduced cell migration and prevented FAO transcriptional activation when combined with alisertib and trametinib. Notably, the ATE triple combination in vivo showed remarkable activity, inducing tumor regression and extensively prolonging mice overall survival. Interestingly, in this study, we corroborated that FAO inhibitors combined with targeted agents prevent the development of acquired drug resistance in *BRAF*-mutant melanoma models (Aloia et al., 2019; Shen et al., 2020). Moreover, we proved that this triple combination is effective also in *NRAS*-mutant advanced melanomas, a particularly difficult clinical setting for which the triple combination may be a potentially pioneering therapeutic tool. These three drugs have already been separately tested in clinical trials, making the repositioning of the combination even more straightforward.

MATERIALS AND METHODS

Animals

NOD.Cg-Prkdc^{scid} Il2rg^{tm1Wjl}/SzJ (NOD scid gamma) mice (aged 4–5 weeks) were purchased from Charles River Laboratories, Wilmington, MA), and breeding was set up in our internal animal facility (Cogentech, Milan, Italy, https://www.cogentech.it/mouse-genetics.php). Male and female mice (aged 7–14 weeks) were

Survival analysis by Kaplan–Meier curves (**$P < 0.01$ by log-rank Mantel–Cox test). AT denotes alisertib and trametinib combination, AT-tum denotes alisertib and trametinib combination–treated tumors, CTR-tum denotes control-treated tumors, Eto denotes etomoxir, ATE denotes etomoxir with alisertib and trametinib treatment, and t0 denotes the start of treatment. CTR, control; FAO, fatty acid oxidation; FC, fold change; GSEA, Gene Set Enrichment Analysis; ns, not significant; po qd × 5 ×3w, per os quaque die (once a day) for 5 days for 3 weeks.

used for experimental procedures and appropriately randomized. In vivo studies were performed after approval from our fully authorized animal facility and notification to the Ministry of Health (as required by Italian law; Institutional Animal Care and Use Committees numbers 758/2015 and 564/2019), in accordance with the Decreto Legislativo 4 Marzo 2014, n. 26, which enforces the Directive 2010/63/EU on the protection of animals used for scientific purposes.

PDXs generation, characterization, and in vitro culture

Metastatic melanoma PDXs were obtained, propagated, and cultured as previously reported (Bossi et al., 2016). For the experiments described in this paper, MM2, MM3, MM13, MM16, MM23, and MM27 PDXs (passage 2, PDX2) were used for ex vivo and in vivo genetic screenings, validation, and drug combination studies (Supplementary Figure S1a).

shRNA-barcoded Libraries design and composition

Actionable and non targeting custom shRNA genetic libraries were constructed as detailed in Supplementary Materials and Methods.

Ex vivo transwell-based migration genetic screen assay

The screens were performed as detailed in Supplementary Materials and Methods. Non targeting and actionable differentially distributed BCs (migrated vs. non-migrated cell populations) were scored using an empirical Bayes dispersion shrinkage procedure as implemented in the edgeR package (Robinson et al., 2010), followed by false discovery rate adjustment (false discovery rate < 0.2). Actionable migration screen candidates were defined on the basis of the distribution of BCs log fold change (the ratio of BC frequency in the migrated cell population compared with that in the non-migrated). Gene-wise BCs' distribution shift and significance were estimated using a Wilcoxon rank-sum test under the null hypothesis (H0) of a BC frequency in migrated cells equal to that in non-migrated ones (i.e., H0:log fold change $= 0$). Genes with significant negative shifts ($P < 0.05$) were included in a tier 1 list of genes (shift analysis). Significance was determined by combining BCs *P*-values using Fisher's sumlog method and defining a tier 2 list of genes (combined significance analysis). The list of hits from tier 1 and tier 2 was merged into the final candidate list.

Please refer to Supplementary Materials and Methods for any detail.

Data availability statement

Datasets related to this article can be found at the following link https://www.ncbi.nlm.nih.gov/geo/query/acc.cgi?acc=GSE207645, hosted at Gene Expression Omnibus. Gene Expression Omnibus accession number GSE207645. A reviewer token is available upon request.

ORCIDs

Federica Marocchi: http://orcid.org/0000-0002-5610-5499
Fernando Palluzzi: http://orcid.org/0000-0003-0861-5512
Paola Nicoli: http://orcid.org/0000-0002-6284-1839
Marine Melixetian: http://orcid.org/0000-0002-8454-8262
Giulia Lovati: http://orcid.org/0000-0002-3702-7501
Giovanni Bertalot: http://orcid.org/0000-0002-4862-7705
Salvatore Pece: http://orcid.org/0000-0003-1764-3929
Pier Francesco Ferrucci: http://orcid.org/0000-0001-6255-5851
Daniela Bossi: http://orcid.org/0000-0002-8507-6754
Luisa Lanfrancone: http://orcid.org/0000-0002-4523-3815

CONFLICT OF INTEREST

The authors state no conflict of interest.

ACKNOWLEDGMENTS

The authors wish to thank Stefania D'Atri, Lauretta Levati, and Giandomenico Russo (Istituto Dermopatico dell'Immacolata, Rome, Italy) for providing drug-resistant melanoma cell lines; Jole Costanza (Fondazione Istituto Nazione di Genetica Molecolare, Milan, Italy) for screen data alignment; Daniel Fernandez Perez (Department of Experimental Oncology, European Institute of Oncology, Milan, Italy) for helpful suggestions and discussion on transcriptomic data analysis; Giuseppe Meroni (Experimental Therapeutics Program, FIRC Institute of Molecular Oncology Foundation, Milan, Italy) for drug resuspension and solubility testing; Alberto Gobbi and Manuela Capillo (Cogentech, Milan, Italy) for the excellent support in mouse work; and the Istituto Europeo di Oncologia Genomic Unit for the considerable technical support. This work was supported by the Associazione Italiana per la Ricerca sul Cancro grant IG 2017 Id 20508 to LL and the Italian Ministry of Health with Ricerca Corrente and 5x1000 funds. FM was supported by Associazione Italiana per la Ricerca sul Cancro (2020) and Fondazione Umberto Veronesi (2023) fellowships. GL was supported by a Fondazione Istituto Europeo di Oncologia Centro Cardiologico Monzino fellowship (2021–2022).

AUTHOR CONTRIBUTIONS

Conceptualization: FM, LL; Data Curation: FM, FP, MM, GL; Formal Analysis: FP, MM; Funding Acquisition: LL; Investigation: FM, PN, GB, SP, PFF, DB, GL; Methodology: FM, FP; Project Administration: FM, LL; Resources: PFF, LL; Software: FP; Supervision: LL; Validation: FM; Visualization: FM, LL: Writing – Original Draft Preparation: FM, LL; Writing – Review and Editing: FM, LL

SUPPLEMENTARY MATERIAL

Supplementary material is linked to the online version of the paper at www.jidonline.org, and at https://doi.org/10.1016/j.jid.2023.03.1665.

REFERENCES

Alkaraki A, McArthur GA, Sheppard KE, Smith LK. Metabolic plasticity in melanoma progression and response to oncogene targeted therapies. Cancers (Basel) 2021;13:5810.

Aloia A, Müllhaupt D, Chabbert CD, Eberhart T, Flückiger-Mangual S, Vukolic A, et al. A fatty acid oxidation-dependent metabolic shift regulates the adaptation of BRAF-mutated melanoma to MAPK inhibitors. Clin Cancer Res 2019;25:6852–67.

Ascierto PA, Ferrucci PF, Fisher R, Del Vecchio M, Atkinson V, Schmidt H, et al. Dabrafenib, trametinib and pembrolizumab or placebo in BRAF-mutant melanoma. Nat Med 2019;25:941–6.

Bossi D, Cicalese A, Dellino GI, Luzi L, Riva L, D'Alesio C, et al. In vivo genetic screens of patient-derived tumors revealed unexpected frailty of the transformed phenotype. Cancer Discov 2016;6:650–63.

Brahmer JR, Lacchetti C, Schneider BJ, Atkins MB, Brassil KJ, Caterino JM, et al. Management of immune-related adverse events in patients treated with immune checkpoint inhibitor therapy: American Society of Clinical Oncology clinical practice guideline. J Clin Oncol 2018;36:1714–68.

Caino MC, Seo JH, Aguinaldo A, Wait E, Bryant KG, Kossenkov AV, et al. A neuronal network of mitochondrial dynamics regulates metastasis. Nat Commun 2016;7:13730.

Caporali S, Alvino E, Lacal PM, Levati L, Giurato G, Memoli D, et al. Targeting the PI3K/AKT/mTOR pathway overcomes the stimulating effect of dabrafenib on the invasive behavior of melanoma cells with acquired resistance to the BRAF inhibitor. Int J Oncol 2016;49:1164–74.

Caporali S, Alvino E, Lacal PM, Ruffini F, Levati L, Bonmassar L, et al. Targeting the *PTTG1* oncogene impairs proliferation and invasiveness of melanoma cells sensitive or with acquired resistance to the BRAF inhibitor dabrafenib. Oncotarget 2017;8:113472–93.

Caputo E, Miceli R, Motti ML, Taté R, Fratangelo F, Botti G, et al. AurkA inhibitors enhance the effects of B-RAF and MEK inhibitors in melanoma treatment. J Transl Med 2014;12:216.

Chamcheu JC, Roy T, Uddin MB, Banang-Mbeumi S, Chamcheu RN, Walker AL, et al. Role and therapeutic targeting of the PI3K/Akt/mTOR signaling pathway in skin cancer: a review of current status and future trends on natural and synthetic agents therapy. Cells 2019;8:803.

Curti BD, Faries MB. Recent advances in the treatment of melanoma. N Engl J Med 2021;384:2229–40.

Dai M, Al-Odaini AA, Fils-Aimé N, Villatoro MA, Guo J, Arakelian A, et al. Cyclin D1 cooperates with p21 to regulate TGFbeta-mediated breast

cancer cell migration and tumor local invasion [published correction appears in Breast Cancer Res 2017;19:43] Breast Cancer Res 2013;15:R49.

Davis SL, Robertson KM, Pitts TM, Tentler JJ, Bradshaw-Pierce EL, Klauck PJ, et al. Combined inhibition of MEK and aurora A kinase in KRAS/PIK3CA double-mutant colorectal cancer models. Front Pharmacol 2015;6:120.

de la Mare JA, Jurgens T, Edkins AL. Extracellular Hsp90 and TGFbeta regulate adhesion, migration and anchorage independent growth in a paired colon cancer cell line model. BMC Cancer 2017;17:202.

de Weger VA, de Jonge M, Langenberg MHG, Schellens JHM, Lolkema M, Varga A, et al. A phase I study of the HDM2 antagonist SAR405838 combined with the MEK inhibitor pimasertib in patients with advanced solid tumours. Br J Cancer 2019;120:286–93.

Diaz JE, Ahsen ME, Schaffter T, Chen X, Realubit RB, Karan C, et al. The transcriptomic response of cells to a drug combination is more than the sum of the responses to the monotherapies. ELife 2020;9:e52707.

Do TV, Xiao F, Bickel LE, Klein-Szanto AJ, Pathak HB, Hua X, et al. Aurora kinase A mediates epithelial ovarian cancer cell migration and adhesion. Oncogene 2014;33:539–49.

Du R, Huang C, Liu K, Li X, Dong Z. Targeting AURKA in Cancer: molecular mechanisms and opportunities for Cancer therapy. Mol Cancer 2021;20:15.

Dummer R, Long GV, Robert C, Tawbi HA, Flaherty KT, Ascierto PA, et al. Randomized phase III trial evaluating spartalizumab plus dabrafenib and trametinib for BRAF V600-mutant unresectable or metastatic melanoma. J Clin Oncol 2022;40:1428–38.

Ferrucci PF, Di Giacomo AM, Del Vecchio M, Atkinson V, Schmidt H, Schachter J, et al. KEYNOTE-022 part 3: a randomized, double-blind, phase 2 study of pembrolizumab, dabrafenib, and trametinib in BRAF-mutant melanoma [published correction appears in J Immunother Cancer 2021;9:e001806corr1] J Immunother Cancer 2020;8:e001806.

Garcia-Alvarez A, Ortiz C, Muñoz-Couselo E. Current perspectives and novel strategies of NRAS-mutant melanoma. Onco Targets Ther 2021;14:3709–19.

González-Ruiz L, González-Moles MÁ, González-Ruiz I, Ruiz-Ávila I, Ayén Á, Ramos-García P. An update on the implications of cyclin D1 in melanomas. Pigment Cell Melanoma Res 2020;33:788–805.

Gutzmer R, Stroyakovskiy D, Gogas H, Robert C, Lewis K, Protsenko S, et al. Atezolizumab, vemurafenib, and cobimetinib as first-line treatment for unresectable advanced BRAFV600 mutation-positive melanoma (IMspire150): primary analysis of the randomised, double-blind, placebo-controlled, phase 3 trial [published correction appears in Lancet 2020;396:466] Lancet 2020;395:1835–44.

Jenkins RW, Fisher DE. Treatment of advanced melanoma in 2020 and beyond. J Invest Dermatol 2021;141:23–31.

Koedoot E, Fokkelman M, Rogkoti VM, Smid M, van de Sandt I, de Bont H, et al. Uncovering the signaling landscape controlling breast cancer cell migration identifies novel metastasis driver genes. Nat Commun 2019;10:2983.

Larkin J, Chiarion-Sileni V, Gonzalez R, Grob JJ, Rutkowski P, Lao CD, et al. Five-year survival with combined nivolumab and ipilimumab in advanced melanoma. N Engl J Med 2019;381:1535–46.

Li X, Seebacher NA, Garbutt C, Ma H, Gao P, Xiao T, et al. Inhibition of cyclin-dependent kinase 4 as a potential therapeutic strategy for treatment of synovial sarcoma. Cell Death Dis 2018;9:446.

Long GV, Hauschild A, Santinami M, Atkinson V, Mandalà M, Chiarion-Sileni V, et al. Adjuvant dabrafenib plus trametinib in Stage III BRAF-mutated melanoma. N Engl J Med 2017;377:1813–23.

Ma J, Wang H, Guo S, Yi X, Zhao T, Liu Y, et al. A20 promotes melanoma progression via the activation of Akt pathway. Cell Death Dis 2020;11:794.

Margue C, Philippidou D, Kozar I, Cesi G, Felten P, Kulms D, et al. Kinase inhibitor library screening identifies synergistic drug combinations effective in sensitive and resistant melanoma cells. J Exp Clin Cancer Res 2019;38:56.

Moreira A, Heinzerling L, Bhardwaj N, Friedlander P. Current melanoma treatments: where do we stand? Cancers (Basel) 2021;13:221.

Nair NU, Das A, Rogkoti VM, Fokkelman M, Marcotte R, de Jong CG, et al. Migration rather than proliferation transcriptomic signatures are strongly associated with breast cancer patient survival. Sci Rep 2019;9:10989.

Pathria G, Garg B, Borgdorff V, Garg K, Wagner C, Superti-Furga G, et al. Overcoming MITF-conferred drug resistance through dual AURKA/MAPK targeting in human melanoma cells. Cell Death Dis 2016;7:e2135.

Puig-Butille JA, Vinyals A, Ferreres JR, Aguilera P, Cabré E, Tell-Martí G, et al. AURKA overexpression is driven by FOXM1 and MAPK/ERK activation in melanoma cells harboring BRAF or NRAS mutations: impact on melanoma prognosis and therapy. J Invest Dermatol 2017;137:1297–310.

Qin G, Xu F, Qin T, Zheng Q, Shi D, Xia W, et al. Palbociclib inhibits epithelial-mesenchymal transition and metastasis in breast cancer via c-Jun/COX-2 signaling pathway. Oncotarget 2015;6:41794–808.

Rambow F, Rogiers A, Marin-Bejar O, Aibar S, Femel J, Dewaele M, et al. Toward minimal residual disease-directed therapy in melanoma. Cell 2018;174:843–55.e19.

Robert C, Grob JJ, Stroyakovskiy D, Karaszewska B, Hauschild A, Levchenko E, et al. Five-year outcomes with dabrafenib plus trametinib in metastatic melanoma. N Engl J Med 2019;381:626–36.

Robinson MD, McCarthy DJ, Smyth GK. edgeR: a Bioconductor package for differential expression analysis of digital gene expression data. Bioinformatics 2010;26:139–40.

Rossi FA, Enriqué Steinberg JH, Calvo Roitberg EH, Joshi MU, Pandey A, Abba MC, et al. USP19 modulates cancer cell migration and invasion and acts as a novel prognostic marker in patients with early breast cancer. Oncogenesis 2021;10:28.

Sarwar M, Syed Khaja AS, Aleskandarany M, Karlsson R, Althobiti M, Ødum N, et al. The role of PIP5K1α/pAKT and targeted inhibition of growth of subtypes of breast cancer using PIP5K1α inhibitor. Oncogene 2019;38:375–89.

Schadendorf D, van Akkooi ACJ, Berking C, Griewank KG, Gutzmer R, Hauschild A, et al. Melanoma [published correction appears in Lancet 2019;393:746] Lancet 2018;392:971–84.

Schuler M, Zimmer L, Kim KB, Sosman JA, Ascierto PA, Postow MA, et al. Phase Ib/II trial of ribociclib in combination with binimetinib in patients with NRAS-mutant melanoma. Clin Cancer Res 2022;28:3002–10.

Shen S, Faouzi S, Souquere S, Roy S, Routier E, Libenciuc C, et al. Melanoma persister cells are tolerant to BRAF/MEK inhibitors via ACOX1-mediated fatty acid oxidation. Cell Rep 2020;33:108421.

Simiczyjew A, Pietraszek-Gremplewicz K, Dratkiewicz E, Podgórska M, Matkowski R, Ziętek M, et al. Combination of selected MET and EGFR inhibitors decreases melanoma cells' invasive abilities. Front Pharmacol 2019;10:1116.

Su B, Gao L, Baranowski C, Gillard B, Wang J, Ransom R, et al. A genome-wide RNAi screen identifies FOXO4 as a metastasis-suppressor through counteracting PI3K/AKT signal pathway in prostate cancer. PLoS One 2014;9:e101411.

Tajadura-Ortega V, Garg R, Allen R, Owczarek C, Bright MD, Kean S, et al. An RNAi screen of Rho signalling networks identifies RhoH as a regulator of Rac1 in prostate cancer cell migration. BMC Biol 2018;16:29.

Tolcher AW, Peng W, Calvo E. Rational approaches for combination therapy strategies targeting the MAP kinase pathway in solid tumors. Mol Cancer Ther 2018;17:3–16.

Vallejo A, Perurena N, Guruceaga E, Mazur PK, Martinez-Canarias S, Zandueta C, et al. An integrative approach unveils FOSL1 as an oncogene vulnerability in KRAS-driven lung and pancreatic cancer. Nat Commun 2017;8:14294.

van Roosmalen W, Le Dévédec SE, Golani O, Smid M, Pulyakhina I, Timmermans AM, et al. Tumor cell migration screen identifies SRPK1 as breast cancer metastasis determinant. J Clin Invest 2015;125:1648–64.

Worrall C, Suleymanova N, Crudden C, Trocoli Drakensjö I, Candrea E, Nedelcu D, et al. Unbalancing p53/Mdm2/IGF-1R axis by Mdm2 activation restrains the IGF-1-dependent invasive phenotype of skin melanoma. Oncogene 2017;36:3274–86.

Wu J, Yang L, Shan Y, Cai C, Wang S, Zhang H. AURKA promotes cell migration and invasion of head and neck squamous cell carcinoma through regulation of the AURKA/Akt/FAK signaling pathway. Oncol Lett 2016;11:1889–94.

Xie L, Meyskens FL Jr. The pan-Aurora kinase inhibitor, PHA-739358, induces apoptosis and inhibits migration in melanoma cell lines. Melanoma Res 2013;23:102–13.

Yang J, Fan J, Li Y, Li F, Chen P, Fan Y, et al. Genome-wide RNAi screening identifies genes inhibiting the migration of glioblastoma cells. PLoS One 2013;8:e61915.

Yang X, Shen H, Buckley B, Chen Y, Yang N, Mussell AL, et al. NTRK1 is a positive regulator of YAP oncogenic function. Oncogene 2019;38:2778–87.

Yu C, Liu X, Yang J, Zhang M, Jin H, Ma X, et al. Combination of immunotherapy with targeted therapy: theory and practice in metastatic melanoma. Front Immunol 2019;10:990.

Zhang G, Frederick DT, Wu L, Wei Z, Krepler C, Srinivasan S, et al. Targeting mitochondrial biogenesis to overcome drug resistance to MAPK inhibitors. J Clin Invest 2016;126:1834–56.

SUPPLEMENTARY MATERIALS AND METHODS

Cell lines

Human embryonic kidney 293T cell line was maintained in DMEM (Euroclone, Pero, Italy, catalog number ECM0103L) with 100 U/ml penicillin and 100 μg/ml streptomycin, supplemented with 10% fetal bovine serum (South American origin, Microtech, Palermo, Italy, catalog number 377664). A375 and SKMEL28 parental and resistant cell lines (A375-P, A375-R, SKMEL28-P, and SKMEL28-R; kindly provided by S. D'Atri and G. Russo, Istituto Dermopatico dell'Immacolata, Istituto di Ricovero e Cura a Carattere Scientifico, Rome, Italy [Caporali et al., 2017, 2016]) were maintained in RPMI-1640 medium (Euroclone, catalog number ECM2001L) supplemented as reported earlier. Resistant cell lines (A375-R, SKMEL28-R) were maintained in culture under selective drug pressure (1.5 μM dabrafenib and 40 nM trametinib).

Short hairpin RNA—barcoded libraries design and composition

Actionable and nontargeting custom short hairpin RNA (shRNA) libraries were constructed using chip-based oligonucleotide synthesis and cloned into the pRSI16-U6-(sh)-UbiC-TagRFP-2A-Puro lentiviral vector as a pool (Cellecta, Mountain View, CA). Actionable library contains 874 vectors, targeting 77 human genes (10 shRNAs per gene), two neutral controls (luciferase, 20 shRNAs per gene; Arietis control scramble, 44 shRNAs), and four positive controls (PSMA1, RPL30, PCNA, POLR2B, 10 shRNAs per gene). Every construct carries a barcode (BC) cassette of 22 degenerated, nonoverlapping nucleotides, univocally associated with each shRNA. The nontargeting library consists of 1,200 vectors, each carrying a unique BC and no associated shRNA.

Drugs for in vitro experiments

AURKA inhibitor alisertib (MLN8237, number S1133) and CDK4/6 inhibitor palbociclib (number S1116) were purchased from Selleck Chemicals (Munich, Germany). MAPK/extracellular signal—regulated kinase kinase 1/2 inhibitor trametinib (GSK1120212, catalog number A-1258) and BRAF inhibitor dabrafenib (catalog number A-1220) were purchased from Active Biochem (Hong Kong, China). Inhibitor of mitochondrial beta-oxidation (inhibitor of the carnitine palmitoyltransferase CPT1) etomoxir (HY-50202/cs-3271) was purchased from MedChemExpress (Monmouth Junction, NJ). For in vitro studies, compounds were resuspended in DMSO at 10 mM (alisertib, trametinib), 20 mM (dabrafenib), and 80 mM (etomoxir) stock concentration.

Plasmids

For screen validation, the shRNAs targeting AURKA and CCND1 were synthesized (Sigma-Aldrich, St. Louis, MO) and cloned into pRSI17-U6-(sh)-UbiC-TagGFP-2A-Puro (linearized vector, catalog number SVSHU617-L, Cellecta), following manufacturer instructions. Two shRNA vectors were generated for each gene, separately tested, and then pooled during lentiviral preparation for cell infection: 5′ACCGGCACATACCAAGAGACTTACAAGTTAATATTCATAG CTTGTAGGTCTCTTGGTATGTGTTTT3′ for shAURKA#1, 5′ACCGGGCAGAGAACTGCTATTTATATGTTAATATTCATAG CATATAAGTAGCAGTTCTCTGCTTTT3′ for shAURKA#2, 5′ ACCGGCCGAGAAGCTGTGTATCTATAGTTAATATTCATAGC TGTAGATGCACAGCTTCTCGGTTTT3′ for shCCND1#1, and 5′ACCGGCCACAGATGTGAAGTTTATTTGTTAATATTCATAG CAAATGAACTTCACATCTGTGGTTTT3′ for shCCND1#2. Luciferase gene shRNA was cloned and used as a control (luciferase-targeted shRNA vector: 5′ACCGGCTTCGAA ATGTTCGTTTGGTTGTTAATATTCATAGCAACCGAACGGAC ATTTCGAAGTTTT3′).

Lentiviral transfection and cell infection

Library vectors and validation plasmids were packaged into lentiviral particles to allow genome integration for stable transduction. The human embryonic kidney 293T packaging cells were transfected using either Lipofectamine LTX/PLUS Reagent Kit (Invitrogen, Waltham, MA, catalog number 15338100) and the calcium phosphate method for library vectors and validation plasmids, respectively. Viral particles were produced using second-generation packaging plasmids pMD2.G-VSVG and pCD-NLBH (a generous gift from Colin Goding, Ludwig Cancer Research, Oxford, United Kingdom).

MM13 and MM27 patient-derived xenograft (PDX) cells (PDX2) were infected with lentiviral particles carrying shRNA actionable library vectors (at a multiplicity of infection of ~0.15) or pools of two shRNA targeting single genes (*AURKA*, *CCND1*) (at a multiplicity of infection = 3). Infection was performed for 16 hours in standard medium supplemented with 6 μg/ml polybrene (Sigma-Aldrich), followed by complete medium replacement. Forty-eight hours after infection, cells were selected with 2 μg/ml puromycin for 3 days.

Ex vivo transwell-based migration genetic screen

The migration genetic screen was performed using fibronectin-coated (fibronectin number 11080938001, Roche, Basel, Switzerland, 5 $\mu g/cm^2$ coating the outer part of the membrane) inserts in six-well plates format (8.0-μm pore size, number 353093, Corning, Corning, NY). Actionable and nontargeting library-transduced PDX cells were plated in the upper chamber of the transwells (350,000 cells per transwell; 85,000 cells/cm^2) in serum-free medium, and complete medium was added to the lower chamber (triplicate pools of eight transwells, ~3,000 cells per BC). After 24 hours, the two cell populations were separately collected: nonmigrated cells were recovered from the upper compartment by sequential PBS washes and delicate membrane tip scraping, and migrated cells were recovered by trypsinization of the outer surface of transwells.

Total genomic DNA was extracted using Blood & Tissue Kit (Qiagen, Hilden, Germany, catalog number 69506), following the manufacturer's instructions. Library BCs were PCR amplified and next-generation sequenced, according to the Cellecta User Manual, and the strategy was further optimized to allow for multiplexing of several samples. PCR amplification products were purified with Qiagen PCR Purification Kit (catalog number 28106, Qiagen) and subjected to quality control using the High Sensitivity DNA Assay of Agilent 2100 Bioanalyzer (following the manufacturer's instruction). Illumina-generated sequences (HiSeq-2000/NovaSeq-6000, Illumina, San Diego, CA) were processed, and resulting reads were analyzed using our in-house pipeline (previously described in Bossi et al., 2016).

Ex vivo migration screen validation and migration drug treatments assay

The migration assay was performed using inserts coated with fibronectin (5 μg/cm^2, catalog number 11080938001, Roche) on the outer part of the filter in a 24-well format (8.0 μm pore size, Corning, catalog number 353097). For migration validation, 25,000 MM13 and MM27 AURKA-targeted shRNA and CCND1-targeted shRNA–silenced cells were resuspended in a serum-free medium and plated in the upper chamber (85,000 cells/cm^2). Alternatively, silenced cells were pretreated with Mitomycin C (10 μg/ml final concentration for 2 hours, M0503, Sigma-Aldrich), and migration assay was performed as reported earlier. For pharmacological validation, MM13 and MM27 cells were pretreated for 48 hours with increasing doses of alisertib or palbociclib (2–50 μM range). Cells were collected and plated (25,000 cells per transwell; 85,000 cells/cm^2) in a serum-free medium. For combination treatment, PDX cells were pretreated with alisertib (500 nM) or dabrafenib (25 nM) for 48 hours. Control and treated cells were seeded in transwells (25,000 MM13 and MM27 cells; 100,000 MM16; 70,000 MM2; 60,000 MM23; and MM3 cells per transwell), and 100 nM trametinib and 100 μM etomoxir were added in the upper chamber. In all conditions, complete medium was added to the lower compartment of the transwells. Migrated cells were stained with 0.5% crystal violet solution (50% crystal violet 1%, Sigma-Aldrich, V-5265, 35% ethanol in water) after 24 hours. Four images of each insert were acquired at the EVOS microscope and analyzed with ImageJ software (National Institutes of Health, Bethesda, MD) to estimate the occupied area and calculate the migration rate (compared with the control, luciferase-targeted shRNA/DMSO). For validation experiments, proliferation rate was assessed by manual cell counting of the two recovered cell populations.

In vivo tumor growth genetic screen

MM13 and MM27 PDX cells at passage 2 were infected with the shRNA actionable library at low multiplicity of infection (see the Lentiviral transfection and infection section). A total of 1,000,000 transduced cells were used as reference, whereas 330,000 cells per mouse (400 cells per BC) were injected intradermally in the back of anesthetized NOD scid gamma mice (triplicate). Tumors were collected at 200 mm^3 in volume.

Total genomic DNA was extracted from tumor samples using phenol-chloroform protocol. Briefly, tissue samples were homogenized in tubes (gentle MAC M tubes, number 130-093-236, Miltenyi Biotec, Bergisch Gladbach, Germany) with P1 buffer (50 mM Tris-hydrogen chloride, pH 8.0, 10 mM EDTA, 100 μg/ml RNAse A). Samples were then lysed, adding 1/20 volume of 10% SDS, and passed through a 22-gauge syringe needle. DNA was then purified by phenol:-chloroform extraction and precipitated in isopropanol, washed in 70% ethanol, and resuspended in highly pure water. PCR-BC amplification and preparation of sequencing libraries were performed as reported earlier for ex vivo migration screen. The in vivo tumor growth screen analysis was conducted as reported (Bossi et al., 2016). Briefly, BC frequency was calculated in reference cells (fc) and tumors (ft) by dividing each BC read count by the total number of aligned reads. For each BC, $\log_2$fold change was calculated as the base 2 logarithm of the ft to fc ratio. The median of $\log_2$fold change BC distribution was used as the threshold to define screen hits. A gene was considered a hit with at least 6 out of 10 BCs below the median threshold.

In vivo mice drug treatment

NOD scid gamma mice (female and male mice, aged 7–12 weeks) were intradermally injected with 200,000 MM13 or MM27 cells (1:3 Matrigel Matrix HC, Corning, catalog number 354248, and L15 medium suspension). For each PDX, when tumors reached a volume of 70–80 mm^3 (10–12 days after cell injection), mice were randomized into experimental groups: alisertib (20 mg/kg); trametinib (0.5 mg/kg); etomoxir (20 mg/kg); alisertib and trametinib combination (20 mg/kg alisertib + 0.5 mg/kg trametinib); and alisertib, trametinib, and etomoxir combination (20 mg/kg alisertib + 0.5 mg/kg trametinib + 20 mg/kg etomoxir). Control untreated and control vehicle groups were included in the experiment. Alisertib (number HY-10971/CS-0106), trametinib (number HY-10999/CS-0060), and etomoxir sodium salt (HY-50202A) were purchased from MedChemExpress. Alisertib was suspended in 10% 2-hydroxypropyl-β-cyclodextrin and 1% sodium bicarbonate (in water), trametinib was suspended in 5% Cremophor-EL and 5% PEG 400 (in water), and etomoxir was suspended in water. Drugs were administered daily by oral gavage, 5 days per week for 3 weeks. Drugs were resuspended daily to avoid stocking of prepared drug solutions. Tumor volumes were monitored at least twice a week and annotated together with the mice's body weight. Tumor volume was calculated using the modified ellipsoid formula: 1/2 (length × width^2). Drug activity and tumor regression were evaluated 6 days after the last treatment administration (partial tumor regression defined as 10–50 mm^3 final volume). Mice were killed once the tumor reached 1,000 mm^3 volume or if showing signs of distress. Kaplan–Meier curves were used to assess the mice's overall survival.

Histological analysis of in vivo treated tumors

Histological analyses were performed on MM13 and MM27 in vivo treated tumors with alisertib and trametinib monotherapy or combination. Two mice per group were treated for 5 days (at doses used for the activity experiment, reported earlier), and tumors were collected, formalin fixed, and paraffin embedded (LogosJ Processor, Milestone, Austion, TX). Tissue processing and immunohistochemistry staining were performed according to our standardized protocols. Briefly, 3-μm-thick formalin fixed and paraffin embedded sections were incubated (37 °C overnight), and immunohistochemistry staining was performed using the Bond III IHC Autostainer for full Automated Immunohistochemistry (Leica Biosystems, Wetzlar, Germany). Antigens were unmasked with Tris-EDTA, pH 9.0 (Bond Epitope Retrieval Solution 2, AR9640, Leica Biosystems) and incubated with the following antibodies (diluted with Bond Primary Antibody Diluent, AR9352, Leica): Ki-67 (rabbit polyclonal, clone SP6, ab16667, 1:200, Abcam. Cambridge, United Kingdom), p21 (mouse mAb, clones sx118, M7202, 1:50, DAKO, Glostrup, Denmark), phosphorylated extracellular signal–regulated kinase 1/2 (Thr202/Tyr204, rabbit mAb, number 4370,

1:200, Cell Signaling Technology, Danvers, MA), and phosphorylated AURKA (Thr288, rabbit polyclonal antibody, number 44-1210, 1:100, Invitrogen, Waltham, MA). Samples were stained with BOND IHC Polymer Detection Kit (DS9800) and counterstained using hematoxylin solution (Leica Biosystems).

Pictures of stained sections were acquired with the Aperio ScanScope XT System (Leica Biosystems) and were analyzed and scored by a senior pathologist. The positivity of Ki-67– and p21-stained cells was calculated as the percentage of the total tumor cell number. The intensity score of phosphorylated extracellular signal–regulated kinase 1/2– and phosphorylated AURKA–stained cells was calculated according to the I*P formula: (% cells × maximum intensity) + (% cells × preponderant intensity).

In vitro drug treatment viability assay

In vitro drug sensitivity was assessed by CyQUANT Cell Proliferation Assay (Invitrogen, catalog number C35012), plating cells in 96-well plates (biological triplicate). A375 and SKMEL28 parental/resistant cell lines were plated (1,000 A375-P and SKMEL28-P cells/well; 1,500 SKMEL28-R cells/well; and 3,000 A375-R cells/well) and treated by a single exposure to either vehicle (DMSO) or increasing concentrations of dabrafenib, trametinib, dabrafenib and trametinib combination, and alisertib and trametinib combination for 72 hours. MM27 cells derived from control and alisertib and trametinib in vivo treated tumors cells were plated (1,500 cells/well) and treated by a single exposure to either vehicle (DMSO) or increasing concentrations of alisertib and trametinib combination or etomoxir for 72 hours. Fluorescence signal was acquired with PHERAstar FSX Microplate Reader, and the relative viability (%) was calculated upon normalization to controls (DMSO treated).

In vitro cell proliferation assay

MM13/MM27 AURKA-targeted shRNA and CCND1-targeted shRNA transduced cells (2,000 cells/well in 96-well-plate format, technical quadruplicate) were incubated for 2 (start of treatment, t0), 24, 48, and 72 hours, and proliferation was measured with CyQUANT Cell Proliferation Assay (Invitrogen, catalog number C35012). The experiment was performed in biological duplicate. For each condition and timepoint, cell proliferation rate is expressed as values normalized to corresponding t0 ones.

Cell cycle analysis

MM13 and MM27 cells were treated for 16 hours with alisertib (500 nM) and/or trametinib (100 nM) (biological triplicate). After drug treatment, cells were pulsed for 1 hour for BrdU incorporation (Sigma-Aldrich, catalog number B5002, 330 nM BrdU final concentration). Cells were then harvested and fixed in pure ethanol. Cells were denatured with 2 M hydrogen chloride for 25 minutes, and the reaction was stopped by adding 0.1 M sodium borate, pH 8.5, for 2 minutes. Cells were stained with anti-BrdU (BD Biosciences, San Jose, CA, catalog number 347580) and FITC secondary antibodies and resuspended in a staining solution with propidium iodide and RNaseA. Stained cells were analyzed by FACS (Celesta, BD Bioscience). Analysis was performed using FlowJo analysis software.

Cell apoptosis analysis

MM13/MM27 AURKA-targeted shRNA and CCND1-targeted shRNA transduced cells were harvested, freshly stained with anti-annexinV-phycoerythrin-conjugated antibody (BD Biosciences, catalog number 51-65875X) and resuspended in DAPI solution. Stained cells were analyzed by FACS (Celesta, BD Bioscience). Analysis was performed using FlowJo analysis software.

RNA extraction and qPCR

Total RNA was extracted from silenced/treated PDX cells using the Quick-RNA MiniPrep (catalog number R1055, Zymo Research, Irvine, CA), following the manufacturer's instructions. RNA was reverse transcribed into cDNA using OneScript Plus cDNA synthesis kit (number G236, Abm Industries, San Francisco, CA), following the manufacturer's instructions. qPCR was performed on the QuantStudio 6 Pro ThermoFisher instrument, with Fast-SYBR Green Master mix 2x (catalog number 4385614, Applied Biosystem, Waltham, MA), specific forward and reverse primer mixture (0.4 μM), and 20 ng cDNA per reaction. The relative quantification of gene expression was determined using the 2^{-DCt} method. *RPLP0* was used as a housekeeping gene. The following qPCR primers were used: AURKA forward 5′-GGAATATGCACCACTTGGAACA-3′, AURKA reverse 5′-TAAGACAGGGCATTTGCCAAT-3′, CCDN1 forward 5′-GCTGCGAAGTGGAAACCATC-3′, CCND1 reverse 5′-CCTCCTTCTGCACACATTTGAA-3′, BBOX1 forward 5′-GACTCACCGGAGCATCTGAC-3′, BBOX1 reverse 5′-CCCAGTTGTGTAAGCCACATT-3′, FABP3 forward 5′-GTGGAGTTCGATGAGACAACAGC-3′, FABP3 reverse 5′-TGGTCTCTTGCCCGTCCCATTT-3′, FA2H forward 5′-CATCATGCTGCACTTCGTCA-3′, FA2H reverse 5′-CATAGAGGACGTAGCCCAGG-3′, ACADS forward 5′-GCTCACGTTGGGGAAGAAAG-3′, ACADS reverse 5′-GAAGGCCATGCGATTCTCAG-3′, ACSM5 forward 5′-GCACCTCTACCTGTTCCTCA-3′, ACSM5 reverse 5′-ATCTCTGCTCCTGTGCCATT-3′, ACAD11 forward 5′-GTGCAACCTCTGGCAGAAACTG-3′, ACAD11 reverse 5′-CCTGACCTTTCCGAGTCTGTAC-3′, CPT1A forward 5′-CAGCATATGTATCGCCTCGC-3′, CPT1A reverse 5′-CTGGACACGTACTCTGGGTT-3′, RPLP forward 5′-TTCATTGTGGGAGCAGAC-3′, and RPLP0 reverse 5′-CAGCAGTTTCTCCAGAGC-3′.

Bulk RNA sequencing

MM27 cells were treated for 16 hours with alisertib (500 nM) and/or trametinib (100 nM) (triplicate). Total RNA was extracted as indicated earlier, and quality was verified with the Agilent 2100 Bioanalyzer (RNA 6000 Nano Chip Kit). RNA-sequencing libraries were prepared starting from 1 μg of total RNA, with TruSeq RNA sample preparation kit, version 2 (catalog number 15025063, Illumina, San Diego, CA), following the manufacturer's instructions. Libraries were checked at Agilent 2100 Bioanalyzer (High Sensitivity DNA Assay). Samples were paired-end sequenced, 50 bp length, and 30–35 million reads per sample (Illumina-Novaseq-6000). Contaminating host (mouse) RNA reads were filtered out using xenome tool (Conway et al., 2012), and the remaining sequences were aligned to human genome (hg19, GRCh38) using TopHat2 (version 2.0.9). Read counts of each gene were quantified using HTseq (Kim et al., 2013), and differential analysis was performed using DESeq R/

Bioconductor package (Anders and Huber, 2010). Principal Component Analysis was performed with R Packages (R, version 4.1.0). Differentially expressed genes were scored comparing alisertib-treated, trametinib-treated, and alisertib and trametinib combination–treated samples with control vehicle–treated samples ($|\log_2\text{fold change}| > 1$ and adjusted $P < 0.05$). Differentially expressed genes were analyzed with Gene Ontology term enrichment (DAVID tool, version 6.8 Beta), Ingenuity Pathway Analysis (Ingenuity Systems, www.qiagenbioinformatics, Qiagen, Redwood City, CA), and Gene Set Enrichment Analysis software (version 2.2.0, Hallmarks/ Kyoto Encyclopedia of Genes and Genomes gene sets).

In particular, downregulated genes ($\log_2\text{fold change} < 0$ and adjusted $P < 0.05$) were subjected to Ingenuity Pathway Analysis (Canonical Pathways), and additive score was calculated for significant pathways ($P < 0.05$) to define the additive effect on their downregulation (pathway additive score = $-\log_{10}[P\text{-value}]$ alisertib and trametinib combination/$-\log_{10}[P\text{-value}]$ monotherapies; additive score > 2 indicates additively regulated pathways).

Western blot

MM27 cells were treated for 16 hours with alisertib (500 nM) and/or trametinib (100 nM). PDX cells were lysed in RIPA buffer (50 mM Tris-hydrogen chloride, 150 mM sodium chloride, 1% NP-40, 0.5% sodium deoxycholate, 0.1% SDS) supplemented with a protease and phosphatase inhibitor cocktails (catalog number 11697498001, Roche, and catalog number A32957, Thermo Fisher Scientific, Waltham, MA). Western blotting analysis was performed as previously described (Aladowicz et al., 2020). The following antibodies were used: phosphorylated mTOR (Cell Signaling Technology, 5536), total mTOR (Cell Signaling Technology, 2972), phosphorylated p70 S6 Kinase (T421/S424, Cell Signaling Technology, 9204), total p70 S6 Kinase (Elabscience, Houston, TX, 14275), phosphorylated S6 (Ser235/236, Cell Signaling Technology, 2211), total S6 (Cell Signaling Technology, 2217), phosphorylated eIF2α (Cell Signaling Technology, 3398), and total eIF2α (Cell Signaling Technology, 5324). GAPDH was used as a loading control (Cell Signaling Technology, 2118).

Statistical analysis

Data are presented as mean ± SD of biological triplicates (if not differently indicated in the text). Comparisons between two or more groups were assessed using two-tailed unpaired Student's *t*-test or one-way ANOVA (for multiple comparison), as indicated in figure legends. A $P < 0.05$ and lower was considered significant. For the in vivo experiments, the statistical difference in tumor volume growth rate was assessed by an unpaired *t*-test, and survival experiments were expressed as Kaplan–Meier survival curves and analyzed with a log-rank (Mantel–Cox) test. The drug additive effect was estimated using Bliss methods (excess over bliss score) (Liu et al., 2018).

SUPPLEMENTARY REFERENCES

Aladowicz E, Granieri L, Marocchi F, Punzi S, Giardina G, Ferrucci PF, et al. ShcD binds DOCK4, promotes ameboid motility and metastasis dissemination, predicting poor prognosis in melanoma. Cancers (Basel) 2020;12:3366.

Anders S, Huber W. Differential expression analysis for sequence count data. Genome Biol 2010;11:R106.

Bossi D, Cicalese A, Dellino GI, Luzi L, Riva L, D'Alesio C, et al. In vivo genetic screens of patient-derived tumors revealed unexpected frailty of the transformed phenotype. Cancer Discov 2016;6:650–63.

Caporali S, Alvino E, Lacal PM, Levati L, Giurato G, Memoli D, et al. Targeting the PI3K/AKT/mTOR pathway overcomes the stimulating effect of dabrafenib on the invasive behavior of melanoma cells with acquired resistance to the BRAF inhibitor. Int J Oncol 2016;49:1164–74.

Caporali S, Alvino E, Lacal PM, Ruffini F, Levati L, Bonmassar L, et al. Targeting the *PTTG1* oncogene impairs proliferation and invasiveness of melanoma cells sensitive or with acquired resistance to the BRAF inhibitor dabrafenib. Oncotarget 2017;8:113472–93.

Conway T, Wazny J, Bromage A, Tymms M, Sooraj D, Williams ED, et al. Xenome–a tool for classifying reads from xenograft samples. Bioinformatics 2012;28:i172–8.

Kim D, Pertea G, Trapnell C, Pimentel H, Kelley R, Salzberg SL. TopHat2: accurate alignment of transcriptomes in the presence of insertions, deletions and gene fusions. Genome Biol 2013;14:R36.

Liu Q, Yin X, Languino LR, Altieri DC. Evaluation of drug combination effect using a Bliss independence dose-response surface model. Stat Biopharm Res 2018;10:112–22.

a

PDX ID	Biopsy site	Classification	Patient therapy	Patient outcome
MM2	Lymph Node	BRAF V600E	None	OS = 24 months
MM3	Subcutaneous	triple wt	None	OS = 12 months
MM13	Lymph Node	NRAS Q61L	Radiotherapy	OS>140 months
MM16	Lymph Node	NRAS Q61K	Dacarbazine + Bevacizumab, Radiotherapy	OS = 47 months
MM23	Lymph Node	NRAS Q61R	None	OS = 37 months
MM27	Lymph Node	BRAF V600E	Temozolomide	OS = 11 months

b

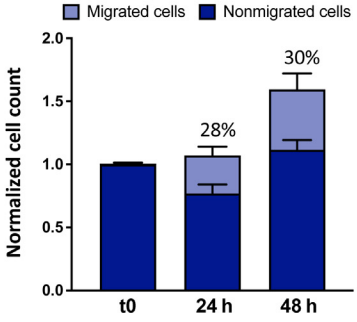

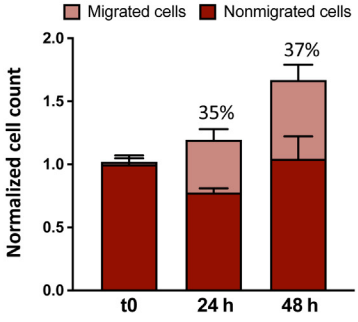

c

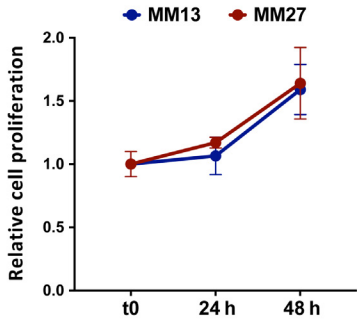

d

Actionable Genes (HUGO gene name)						
ABL1	CCND1	ERBB2	HRAS	MAP4K1	NOTCH2	PTEN
ABL2	CCND2	ERBB3	HSP90AA1	MDM2	NRAS	RAF1
AKT1	CCND3	FGFR1	IDH1	MET	NTRK1	RET
AKT3	CCNE1	FGFR2	IDH2	KMT2A	NTRK2	ROS1
ALK	CDK4	FGFR3	IGF1R	MMP2	NTRK3	SMO
APC	CDK6	FKBP5	KDR	MTOR	PGR	STK4
ATR	CDKN2A	FLT3	KIT	MYD88	PIK3C2B	SYK
AURKA	EGFR	FUS	KRAS	NCOR2	PIK3CA	TAOK1
BRAF	EPHA1	GNA11	MAP2K1	NF1	PIK3CB	TAOK2
BRCA1	EPHA4	HDAC9	MAP3K11	NF2	PIP5K1A	TP53
BRCA2	EPHB2	HGF	MAP3K4	NOTCH1	PRKCZ	TSC1

Library Control Genes					
Luciferase (Luc)	Scramble controls	PSMA1	RPL30	PCNA	POLR2B

Supplementary Figure S1. Metastatic melanoma PDXs are characterized for their migratory capacities and screened with an shRNA library of actionable genes. (**a**) Table reporting the main clinical features of metastatic melanoma PDXs. (**b, c**) PDXs (MM13, MM27) migratory capacities assessment timeline (t0, 24 hours, 48 hours). The migration rate is assessed as the number of migrated cells per total number of recovered cells (normalized cell count); the average migration rate percentage is indicated. (**b**) PDXs (MM13, MM27) proliferation assessment timeline. The proliferation rate is expressed as the total number of recovered cells at each time point (normalized to t0, **c**). (**d**) Actionable library composition: 77 genes (10 shRNA per gene) and 6 control genes. MM, metastatic melanoma; OS, overall survival; PDX, patient-derived xenograft; shRNA, short hairpin RNA.

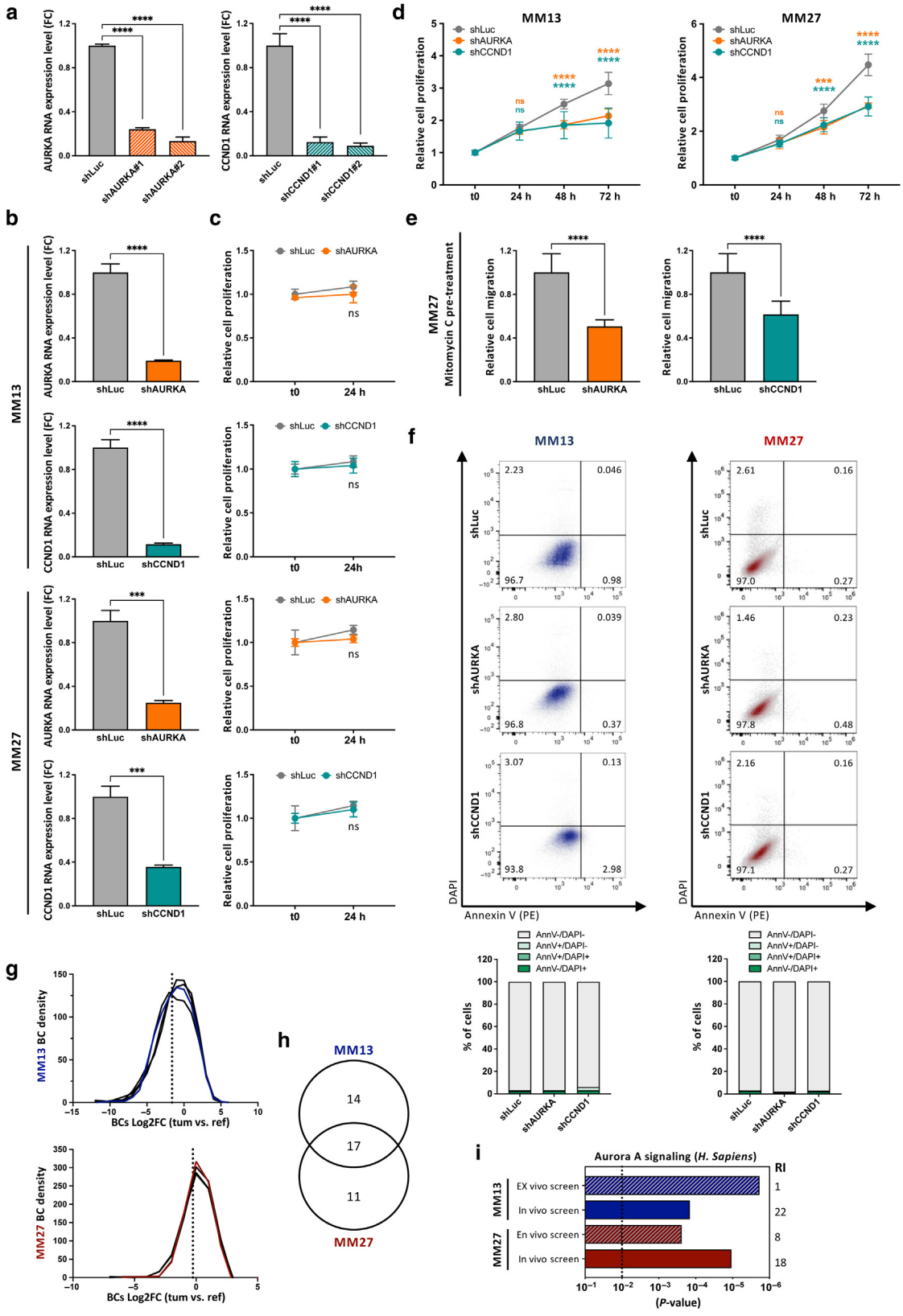

Supplementary Figure S2. Impact of AURKA and CCND1 silencing on PDX cell migration, proliferation, apoptosis, and tumor growth. (**a**) Silencing efficiency of two shRNA vectors per target gene (shAURKA, shCCND1) (A375 cell line, values normalized to those of shLuc; ****$P < 0.0001$ by unpaired *t*-test). (**b**) Silencing efficiency of shAURKA and shCCND1 vector pools in MM13/MM27 cells (values normalized to those of shLuc; ***$P < 0.001$ and ****$P < 0.0001$ by unpaired *t*-test). (**c**) Proliferation rate of shAURKA/shCCND1 MM13/MM27 cells during migration assay (values normalized to t0 values; ns denotes not significant by unpaired *t*-test). (**d**) Cell proliferation of shAURKA and shCCND1 MM13/MM27 cells (CyQuant assay, values normalized to t0 values; ***$P <$ 0.001 and ****$P < 0.0001$ by unpaired *t*-test). (**e**) Effect of AURKA and CCND1 silencing on migratory capacities of Mitomycin C–pretreated MM27 cells

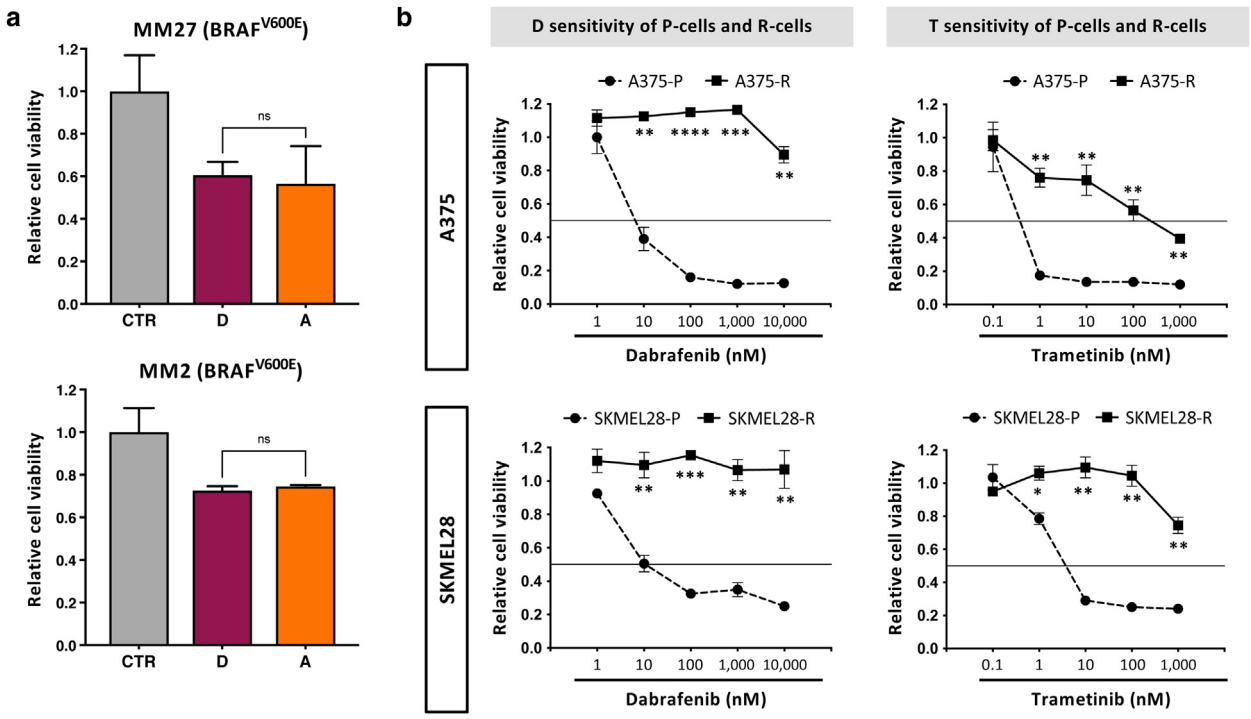

Supplementary Figure S3. A375 and SKMEL28 parental and resistant melanoma cell lines show different sensitivity to dabrafenib and trametinib treatment. (**a**) MM27 and MM2 cell viability upon treatment with alisertib (500 nM) and dabrafenib (10 nM for MM2, 25 nM for MM27) before seeding for transwell migration (values are normalized to those of the CTR; ns denotes not significant by unpaired *t*-test). (**b**) A375 and SKMEL28 parental (P-cells) and resistant (R-cells) cell lines sensitivity to dabrafenib (left) and trametinib (right) monotherapies (CyQuant assay; values are normalized to those of the CTR; $*P < 0.05$, $**P < 0.01$, $***P < 0.001$, and $****P < 0.0001$ by unpaired *t*-test). A, denotes alisertib, and D denotes dabrafenib. CTR, control.

(values normalized to those of shLuc; $****P < 0.0001$ by unpaired *t*-test). (**f**) Apoptosis studies (AnnexinV-DAPI staining) of shAURKA and shCCND1 MM13/MM27 cells. Representative FACS plots and quantification of apoptotic phases are reported. (**g**) BCs density distribution for in vivo actionable screen. Black curves represent single tumor replicates, colored curves represent average distribution, and dotted lines represent the median of the average distribution. (**h**) Venn diagram of common and unique in vivo actionable hits. (**i**) AURKA signaling pathway involvement in the MM13 and MM27 in vivo and ex vivo screens (EnrichR pathway analysis; dotted line indicates $P = 0.01$; combined score-based RI). BC, barcode; PDX, patient-derived xenograft; RI, Ranking Index; shAURKA, AURKA-targeted short hairpin RNA; shCCND1, CCND1-targeted short hairpin RNA; shLuc, luciferase-targeted short hairpin RNA; shRNA, short hairpin RNA.

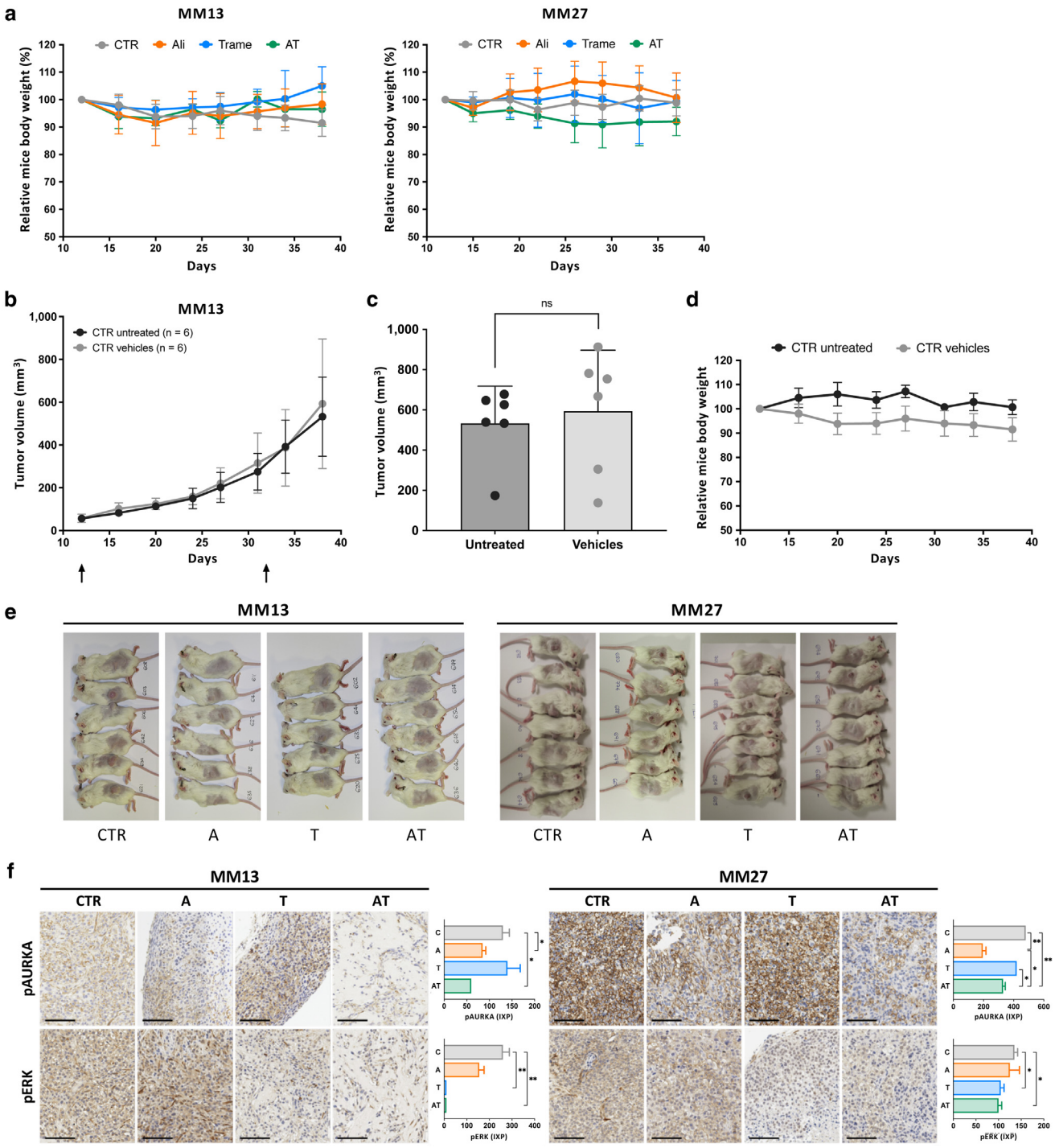

Supplementary Figure S4. Alisertib and trametinib combination is well-tolerated in vivo, additively reduces MM13/MM27 tumor growth, and displays an on-target effect. Assessment of AT activity in vivo in MM13 and MM27 (vehicle, CTR; alisertib, 20 mg/kg; trametinib, 0.5 mg/kg; po qd × 5 × 3w). (**a**) Relative mice body weight. (**b**–**d**) Assessment of the toxicity of drugs vehicles (MM13; CTR untreated vs. CTR vehicles): (**b**) tumor growth curves, (**c**) tumor volume quantification (6 days after last treatment), and (**d**) relative mice body weight. (**e**) Treated mice groups pictures (6 days after the last treatment; related to Figure 4a quantification). (**f**) Immunohistochemistry analysis of MM13- and MM27-treated tumors. Representative images and quantification for pAURKA and pERK are shown (bar = 100 μm; $*P < 0.05$ and $**P < 0.01$ by unpaired *t*-test). AT denotes alisertib and trametinib combination, Ali denotes alisertib, and Trame denotes trametinib. CTR, control; pAURKA, phosphorylated AURKA; pERK, phosphorylated extracellular signal–regulated kinase; po qd × 5 ×3w, per os quaque die (once a day) for 5 days for 3 weeks.

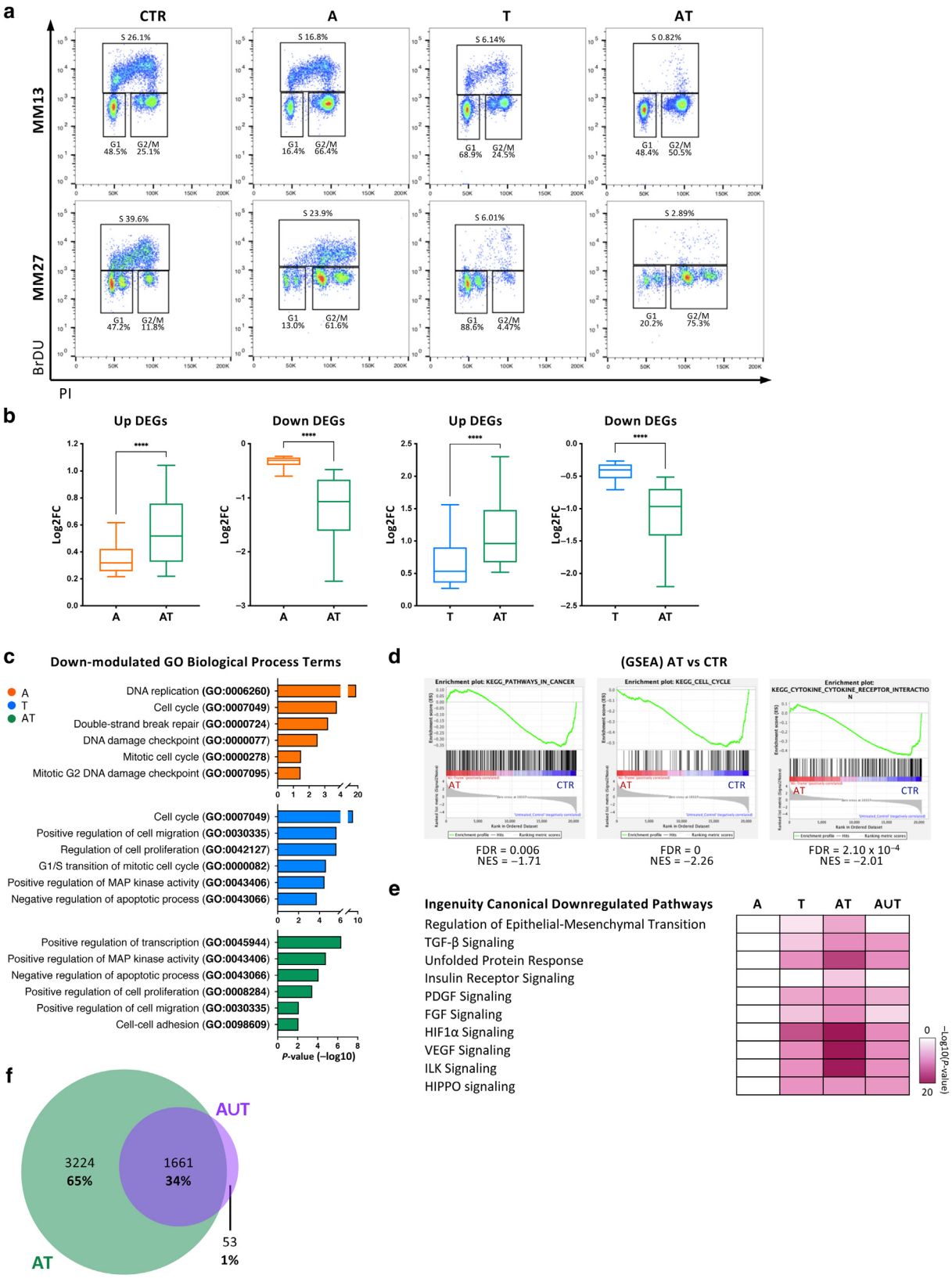

Supplementary Figure S5. Alisertib and trametinib combination regulate specific biological processes and numerous critical cancer pathways. (**a**) Cell cycle analysis (BrdU PI) of AT-treated MM13/MM27 cells. Flow cytometry profiles and corresponding cell percentages are reported. (**b**−**f**) Transcriptomic profile (bulk RNAseq) of MM27 AT-treated cells. Log_2FC distribution of gene expression, for upregulated (up DEGs) and downregulated genes (down DEGs), comparing monotherapies (A, T) and AT combination (****$P < 0.0001$ by unpaired Mann−Whitney test). (**b**) Gene Ontology analysis of AT treatments ($|log_2FC| > 1$, adjusted $P < 0.05$; for A-samples $|log_2FC| > 0.5$, adjusted $P < 0.05$; David Functional Annotation Tool). (**c**) GSEA of AT-treated cells compared with that of CTR (FDR < 0.25). (**d**) Heat map of downmodulated pathways (IPA; adjusted $P < 0.05$ and AS < 2). (**e**) Venn diagram of differentially downmodulated genes for AT

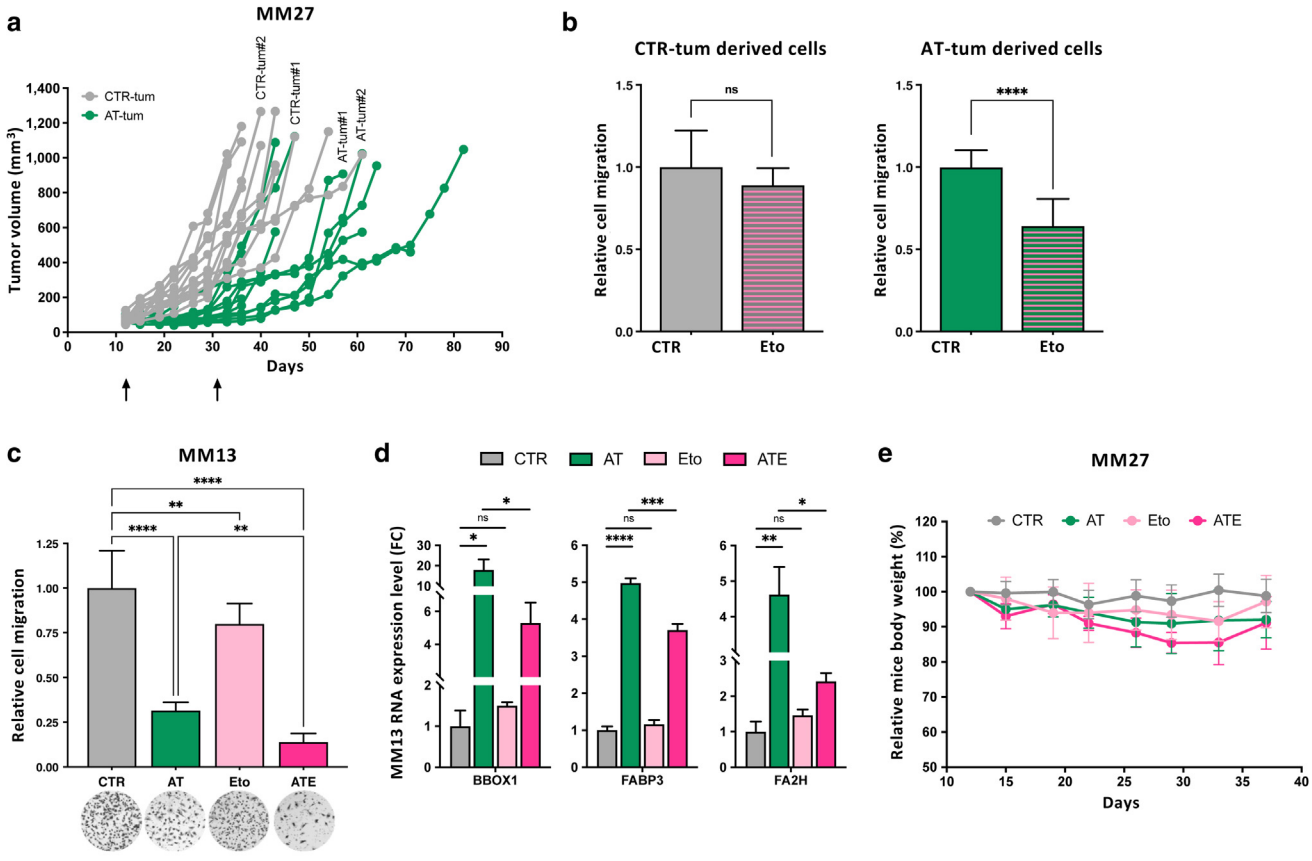

f

Groups *	Tumor Weight Inhibition # (vs CTR)	Tumor regression (% mice) #, §	Tumor growth ^ (median OS, days)	Tumor growth delay (vs CTR, days)	Toxicities (% mice)
CTR	-	0/11	41.5	-	0/12
Alisertib + Trametinib (AT, 20 mg/kg + 0.5 mg/kg)	68.4%	1/11 (9.1%)	59	17.5 (42.2%)	1/12 (8%)
Etomoxir (Eto, 20 mg/kg)	15.2%	0/5	50	8.5 (20.5%)	0/5
Alisertib + Trametinib + Etomoxir (ATE, 20 mg/kg + 0.5 mg/kg + 20 mg/kg)	92.7%	5/7 (71.4%)	95	53.5 (128.9%)	0/7

* treatment schedule: po qdx5x3w; # at 6 days after last treatment; § partial regression (10-50 mm^3 tumor volume);
^ mice were sacrificed at 1,000 mm^3 tumor volume; OS = overall survival

Supplementary Figure S6. ATE triple combination treatment provides additional benefits in melanoma PDXs. (**a**) Tumor growth curves of MM27 AT-treated mice (black arrows indicate treatment administration window, related to Figure 4a). (**b**) Effect of etomoxir treatment on MM27 CTR and AT-tum cells migratory capacities (values are normalized to those of corresponding CTRs; $^{****}P < 0.0001$ by unpaired *t*-test). (**c**) Effect of ATE simultaneous treatment on MM13 migratory capacities ($^{**}P < 0.01$ and $^{****}P < 0.0001$ by one-way ANOVA). (**d**) Transcriptional expression levels of FAO genes upon ATE treatment in MM13 ($^{*}P < 0.05$, $^{**}P < 0.01$, and $^{***}P < 0.001$ by unpaired *t*-test). (**e, f**) Assessment of ATE activity in vivo in MM27. (**e**) Relative mice body weight. (**f**) Summary table (tumor growth inhibition, survival analysis). Eto denotes etomoxir, AT denotes alisertib and trametinib combination, AT-tum denotes alisertib and trametinib combination–treated tumors, and ATE denotes a combination of etomoxir with alisertib and trametinib. CTR, control; FAO, fatty acid oxidation; ns, not significant; PDX, patient-derived xenograft.

and AUT samples (adjusted $P < 0.05$, $\log_2 FC < 0$). (**f**) A denotes alisertib, T denotes trametinib, and AT denotes alisertib and trametinib combination. AS, additive score; CTR, control; DEG, differentially expressed gene; FC, fold change; FDR, false discovery rate; GSEA, Gene Set Enrichment Analysis; IPA, Ingenuity Pathway Analysis; K, thousand; PI, propidium iodide; RNAseq, RNA sequencing.